

NONLINEAR FINITE ELEMENT ANALYSIS OF STEEL PIPE WITH STIFFENER PLATE

Mr. Rut Su

A Thesis Submitted in Partial Fulfillment of the Requirements
for the Degree of Master of Engineering in Civil Engineering
Department of Civil Engineering
Faculty of Engineering
Chulalongkorn University
Academic Year 2018
Copyright of Chulalongkorn University

บทคัดย่อและแฟ้มข้อมูลฉบับเต็มของวิทยานิพนธ์ตั้งแต่ปีการศึกษา 2554 ที่ให้บริการในคลังปัญญาจุฬาฯ (CUIR)
เป็นแฟ้มข้อมูลของนิสิตเจ้าของวิทยานิพนธ์ที่ส่งผ่านทางบัณฑิตวิทยาลัย

The abstract and full text of theses from the academic year 2011 in Chulalongkorn University Intellectual Repository (CUIR)
are the thesis authors' files submitted through the Graduate School.

1413517646
CU Thesisis 6070287021 thesis / recv: 01082562 19:12:57 / seq: 13

6070287021_1413517646

การวิเคราะห์ไฟไนต์อิลิเมนต์ไร้เชิงเส้นของท่อเหล็กที่มีแผ่นเสริมกำลัง

นายรัฐ ชู

วิทยานิพนธ์นี้เป็นส่วนหนึ่งของการศึกษาตามหลักสูตรปริญญาวิศวกรรมศาสตรมหาบัณฑิต
สาขาวิชาวิศวกรรมโยธา ภาควิชาวิศวกรรมโยธา
คณะวิศวกรรมศาสตร์ จุฬาลงกรณ์มหาวิทยาลัย
ปีการศึกษา 2561
ลิขสิทธิ์ของจุฬาลงกรณ์มหาวิทยาลัย



1413517646

CU Thesisis 6070287021 thesis / recv: 01082562 19:12:57 / seq: 13

รัฐ ชู : การวิเคราะห์ไฟไนต์เอลิเมนต์ไร้เชิงเส้นของท่อเหล็กที่มีแผ่นเสริมกำลัง. (NONLINEAR FINITE ELEMENT ANALYSIS OF STEEL PIPE WITH STIFFENER PLATE) อ.ที่ปรึกษาหลัก : ผศ. ดร.เสวกชัย ตั้งอร่ามวงศ์

งานวิจัยชิ้นนี้นำเสนอการใช้วิธีการทางคณิตศาสตร์ในการวิเคราะห์ ท่อเสาเหล็กที่ต่อกับคานซึ่งรับน้ำหนักของครนจากอุตสาหกรรม และใช้แผ่นเหล็กมาทำการเสริมกำลังของเสาให้สามารถรับน้ำหนักมากขึ้นในขณะที่เกิดพฤติกรรมการวิบัติแบบการโก่งเดาะเฉพาะจุด ในงานชิ้นนี้จะพิจารณาถึงคุณสมบัติที่ไร้เชิงเส้นของวัสดุ การขึ้นรูปแบบจำลองของท่อเสาเหล็กรูปสี่เหลี่ยมจัตุรัสจะถูกสร้างเป็นลักษณะสามมิติ ซึ่งใช้อิเล็กเมนต์ไอโซพารามเมตริกสามมิติแบบแปดจุดต่อ โดยนำโปรแกรมวิเคราะห์ไฟไนต์เอลิเมนต์เชิงพาณิชย์ที่เรียกว่า ANSYS มาทำการวิเคราะห์ปัญหาในขนาดและความหนาของเสาที่แตกต่างกัน สำหรับแผ่นเหล็กที่จะนำมาเสริมกำลังจะทำการใช้ความหนาที่แตกต่างกันโดยเขียนรหัสโปรแกรมคอมพิวเตอร์ผ่านโปรแกรม MATLAB ซึ่งสะดวกในการส่งผ่านข้อมูลเข้าไปยัง ANSYS ได้โดยตรง ซึ่งวิธีการเสริมกำลังจะมีทั้งหมดสองรูปแบบได้แก่ การใช้แผ่นเหล็กนำมาเสริมรอบด้านนอกของท่อเสาเหล็ก และการนำแผ่นเหล็กเสริมภายในท่อเสาเหล็ก จากการศึกษาพบว่าพฤติกรรมการโก่งเดาะเฉพาะจุดจะมีอยู่สองรูปแบบได้แก่ การวิบัติบริเวณแรงดึง และการวิบัติบริเวณแรงอัดที่ตำแหน่งขอบบนและขอบล่างของคานที่นำมาเชื่อมต่อกับท่อเสาเหล็ก นอกจากนี้จากการศึกษาพบว่า การใส่แผ่นเหล็กเสริมกำลังจะช่วยเพิ่มขีดจำกัดการรับแรงและยืดขยายอายุการใช้งานของท่อเสาเหล็กได้มากขึ้น วิทยานิพนธ์ฉบับนี้จะสามารถนำเสนอวิธีการออกแบบให้แก่มาตรฐานโครงสร้างสำหรับการก่อสร้างโรงงาน

สาขาวิชา วิศวกรรมโยธา
ปีการศึกษา 2561

ลายมือชื่อนิสิต
ลายมือชื่อ อ.ที่ปรึกษาหลัก

6070287021 : MAJOR CIVIL ENGINEERING

KEYWORD: Nonlinear finite elements, Steel hollow section column,
Elastoplastic materials, Local buckling failures, Steel column
stiffener

Rut Su : NONLINEAR FINITE ELEMENT ANALYSIS OF STEEL PIPE WITH
STIFFENER PLATE. Advisor: Asst. Prof. SAWEKCHAI TANGARAMVONG, Ph.D.

This thesis presents the numerical studies of steel hollow section columns connected to corbels under industry crane loads, and the stiffening design using steel plates to enhance the maximum loading capacity against premature local buckling failures. The influences of inelastic material properties and geometry nonlinearity on the overall load carrying capacity of the columns were considered. Square hollow section columns were modelled in 3D using standard eight-node solid finite elements using an ANSYS software. The plate stiffener design algorithm involving variation of plate thicknesses was coded in MATLAB with a direct application programming interface to ANSYS. The full history of elastoplastic structural responses of the column was mapped out, and described its intrinsic local buckling behaviors at the contact forces. In essence, this study showed the two major tension and compression failures associated with the slendernesses of column section. Two strengthening techniques, namely external ring stiffener and internal plate fabrication, were proposed to extend the overall load carrying capacity and hence the service life of the column. The applications of the proposed analysis and design schemes were illustrated through standard warehouse structures.

Field of Study: Civil Engineering

Student's Signature

Academic Year: 2018

Advisor's Signature



1413517646

CD :Thesis 6070287021 thesis / rev: 01082562 19:12:57 / seq: 13

ACKNOWLEDGEMENTS

My thesis finished by supporting of main three parts. Firstly, I would like to express my sincere thanks to my thesis advisor, Assist. Prof. Dr. Sawekchai Tangaramvong for his invaluable help and constant encouragement throughout the course of this research. I would not have achieved this far and this thesis would not have been completed without all the support that I have always received from him. Secondly, thank you for my parents and my friends for all their support throughout the period of this research. Finally, the authors gratefully acknowledge the support provided by Pacific Pipe Public Company under the research collaboration scheme and financial support from Chulalongkorn University through Applied Mechanics and Structure Research Unit.

Rut Su

TABLE OF CONTENTS

	Page
ABSTRACT (THAI)	iii
ABSTRACT (ENGLISH)	iv
ACKNOWLEDGEMENTS	v
TABLE OF CONTENTS	vi
CHAPTER 1 INTRODUCTION	1
1. Background and Motivation.....	1
2. Research Objective.....	4
3. Scope of Research.....	4
4. Research Significant and Innovative	4
5. Research Design and Methodology.	5
CHAPTER 2 LITERATURE RESEARCH.....	6
1. Crane loads and Joint Detail.....	6
1.1 Typical Runway Crane Load.	6
1.2 Connection Detail	8
1.3 Beam to column connection	10
2. Von-Mises Stress	11
2.1 Definition of Yield strength	11
2.2 Index Notations	13
2.3 Maximum Distortion Energy Theory (von Mises yield criterion).....	14
3. Finite element.....	15
3.1 Introduction.....	15

3.2 SOLID185 Homogeneous Structural Solid Element Description.....	16
4. Cold-Formed Structural Steels.....	16
4.1 General Remark.....	16
4.2 Local Buckling of Columns.....	18
4.3 Inelastic Buckling Analysis.....	19
4.4 Design Concept of Structural Steel Members.....	20
4.5 Column plastification.....	24
5. Non-linear analysis for estimating limit loads.....	25
5.1 Arc-length method.....	25
6. Stiffened Tubular T-joint connection.....	28
6.1 Introduction.....	28
6.2 Internal plate strengthening technique.....	29
6.3 External ring strengthening technique.....	31
CHAPTER 3 METHODOLOGY.....	34
1 Finite Element Modelling of Column and Connection Structures.....	34
1.1 Material properties.....	34
1.2 Geometry.....	34
1.3 Finite Element Types and Discrete Structural Model.....	35
1.4 Load and Boundary Conditions.....	36
2. Plastic Analysis Implementation.....	37
2.1 Non-linear Finite Element Analysis.....	37
3. Retrofit of Hollow-Section Columns.....	38
3.1 Internal Plate Fabrication Strengthening.....	38
3.2 External Ring Stiffener Strengthening.....	39



1413517646

CD :Thesis 6070287021 thesis / recv: 01082562 19:12:57 / seq: 13

CHAPTER 4 Results and Discussions 40

 4.1 Comparison of Numerical Results with Experimental reference..... 40

 4.2 Results before strengthening 40

 4.3 Results for Internal Plate Fabrication..... 43

 4.4 Results for External Ring Stiffener..... 49

 4.5 Summary of Results..... 55

CHAPTER 5 Conclusion 58

REFERENCES 59

VITA..... 66

CHAPTER 1 INTRODUCTION

1. Background and Motivation.

Design of steel structures is a combinatorial process between architecture, safety and integrity. Good design complies with various performance criteria posed by all stakeholders at optimal resources. The design of steel hollow structural section (HSS) members has gained popularity among designers. The close section geometry enhances its ability to behave well under compression as well as its combination with flexural and torsion forces, whilst it only costs the minimum self-weight. In view of strength consideration, the steel hollow sections as depicted in Figure 1.1. Wardenier, Packer et al. (2002) provide the higher load capacity than the open sections. Such physical property has made the steel hollow sections suitably employed for various structures and infrastructures, especially those with some special requirements as long-span capability.

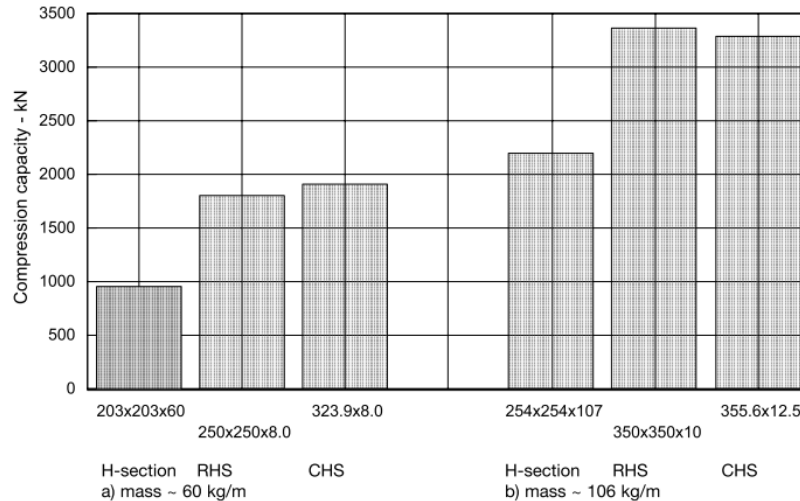


Figure 1.1 Comparison of compression capacity for sections of equal mass (Kurobane 2004).

One of the main drawbacks that unfortunately limits the general usage of steel hollow sections is the occurrence of physically instabilizing local buckling failures under concentrated forces. A specific example is a steel HSS column with corbel supporting heavily industry crane loads of warehouses. The thin surface of HSS

members has made itself prone to the premature failure caused by the eccentrically applied loads.

The intrinsic behaviors of steel sections undergoing local buckling phenomena are rather sporadic. These have yet been precisely described by standard mathematical formulations. The approximate or empirical based equations were developed for local buckling responses of steel open sections under compression and/or flexural forces, as well as their strengthening procedures to enhance the overall member capacity. However, both the response equations and strengthening methods have yet been maturely studied for the steel hollow sections. Whilst some strengthening techniques using steel plates welded to the main column are implemented by individuals' experience, only limited works on the intrinsic behaviors and (at least numerical) justification are systematically available.

The aforementioned comments motivate the work presented herein. In essence, the thesis proposes the nonlinear numerical analysis and design using 3D finite element (FE) methods to describe the behaviors of steel HSS columns under intensively applied forces. Two strengthening techniques using steel plates, namely internal and external fabrications, were studied. The applications of the proposed analysis and retrofitting design methods are illustrated through the steel columns with corbel supporting industry crane loads, usually designed for standard warehouses.

The outline of the thesis is as follows. In the next Chapter 2, the literature reviews on the design standards prescribing the column stiffening techniques are provided. Chapter 3 then implemented the nonlinear 3D FE analyses of various steel HSS columns under crane load. The design and analysis of unstiffened and stiffened columns with steel plates were implemented using the commercial FE analysis software, called ANSYS. A simple design algorithm was coded in MATLAB environment to appropriately adjust stiffening plate properties. The analysis and

design results are reported and discussed in Chapter 4. Finally, concluding remarks are drawn in Chapter 5.



1413517646

CU iThesis 6070287021 thesis / recv: 01082562 19:12:57 / seq: 13

2. Research Objective.

The two main objectives of the present research are

- (1) To investigate the intrinsic behavior of the hollow steel columns supporting heavily loaded cranes, which consider as static forces by performing non-linear stress analysis.
- (2) To suggest the stiffening design model of the hollow steel columns that can safety support the heavily loaded cranes.

3. Scope of Research.

- (1) The material employed cold formed steel with Square Hollow Section.
- (2) Chord width ratio (β) between column and beam connection are equal to 1.
- (3) Perform stress analysis by using plastic hinge concept confined safety at Nodal point, which considered as a 3D Solid model.
- (4) Stiffen the steel column with the plate and standard of steel is TIS SS400.
- (5) Consider the industry-purpose crane load as static forces.
- (6) Grade of steel to consider is TIS SS400 and ASTM A36 with yield stress is equal to 235 and 250 MPa, respectively.
- (7) Size of Geometry was selected from standard steel profiles in the company.
- (8) The effects of residual stress and initial crookedness are ignored.

4. Research Significant and Innovative.

This research performs nonlinear analysis considering elastic perfectly plastic material properties between connection of the column and beam connection. The complex geometry can be analyzed automatically by using commercial finite element software and computational languages. Then perform the safety assessment and stiffened joints using the plastic analysis method.



1413517646

CD IThesis 6070287021 thesis / recv: 01082562 19:12:57 / seq: 13

5. Research Design and Methodology.

(1) Equivalent Static Load Calculation.

For the intensive crane load we can simplify as a static load by calculated the maximum wheel load in each side of the crane, since the bridge girder of the crane have two wheels then we can multiply the wheel load by two and applied maximum wheel load on the geometry.

(2) Stress analysis of 3D Hollow-Section Column with corbel under crane load.

Perform 3D finite element analysis with eight nodes solid element. Non-linear with large deformation is used in the model Aim of this part is study behavior at the connection between column and corbel under the maximum static wheel load. The geometry of column to model in finite element program will be use in catalog from company.

(3) Design of column strengthening.

Since to local buckling occurred at the connection between column and corbel. We need to improve the stiffness of this hollow steel column to insure against local buckling. Perform the safety assessment and stiffened joints using the stress analysis with 2 designs of stiffened model that can improve strength of hollow steel columns called internal plate fabrication and external ring stiffener. For both of strengthening technique with stiffener plate, perform non-linear analysis by changing the thickness of stiffener plate. The results are plotted in load-deflection curve by tracking the displacement at the end of braced member.

CHAPTER 2 LITERATURE RESEARCH.

1. Crane loads and Joint Detail.

1.1 Typical Runway Crane Load.

Crane Load can be determined according to MBMA (2012), columns that affected by crane loads must be designed to resist the loads and prevent the local or global buckling. The detail of the EOT crane on a corbel can be represented with Figure 2.1. The following main loads are needed to determine:

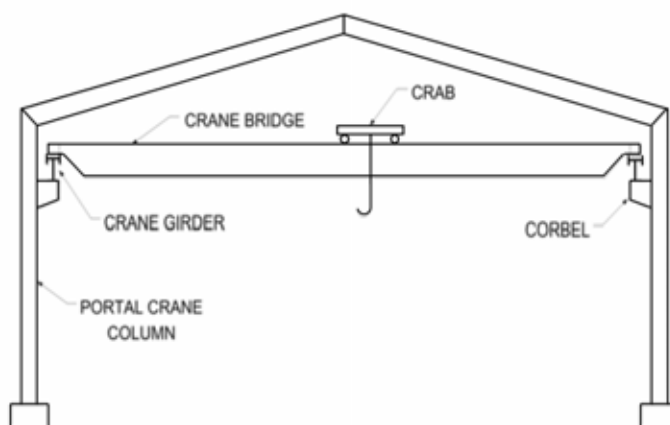


Figure 2.1 The portal frame with the EOT crane on a corbel (Thompson 2007).

1.1.1 Vertical Force:

The vertical force can be considered as wheel load. The magnitude of wheel load will occur when the crane is lifting its rated capacity load. This load may differ from wheel to wheel, depending on the relative positions of the crane components and the lifted load. When the maximum wheel load is not specified for bridge cranes with hook type hoists, it may be conservatively approximated from the crane loads as follows:

$$WL = \frac{RC + HT + 0.5CW}{NW_b}$$

Where

WL = Maximum wheel load.

RC = Rated capacity of the crane.

HT = Weight of hoist with trolley.



CW = Weight of the crane excluding the hoist with trolley.

NW_b = Number of end truck wheels at one end of the bridge.

1.1.2 Lateral Force:

The lateral force on bridge crane runway beams shall be calculated as 20 percent of the sum of the rated capacity of the crane and the weight of the hoist and trolley. The lateral force can be considered to act horizontally at the traction surface of a runway beam.

1.1.3 Longitudinal Force:

Runway beams, including monorails, their connections, and the longitudinal bracing system shall be designed to support horizontal forces calculated as 10 percent of the maximum wheel loads excluding vertical impact. Longitudinal forces shall be assumed to act horizontally at the top of the rails and in each direction parallel to each runway beam (MBMA 2012).

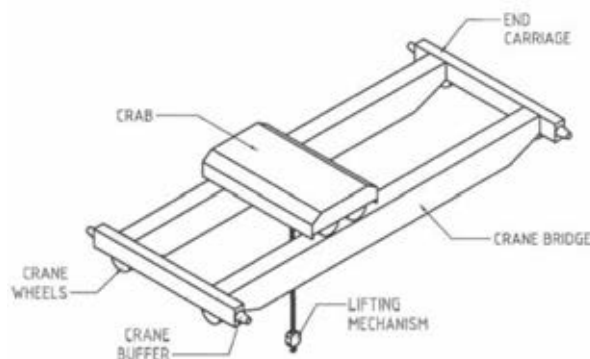


Figure 2.2 The main component of EOT cranes (Thompson 2007).

1.1.3 Crane Loading Conditions

From MBMA (2012), location and lateral movement of the trolley can have some influence to the maximum wheel load. Crane loading condition can be shown in Figure 2.3 including the following four conditions:

- (1) The maximum wheel load at the left end truck and the minimum wheel load at the right end truck, acting simultaneously with the lateral force acting to the left.

- (2) The maximum wheel load at the left end truck and the minimum wheel load at the right end truck, acting simultaneously with the lateral force acting to the right.
- (3) The maximum wheel load at the right end truck and the minimum wheel load at the left end truck, acting simultaneously with the lateral force acting to the left.
- (4) The maximum wheel load at the right end truck and the minimum wheel load at the left end truck, acting simultaneously with the lateral force acting to the right.

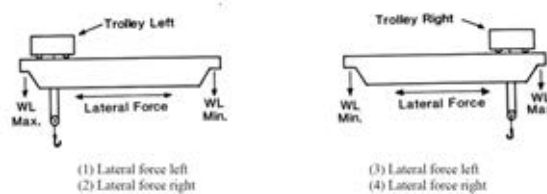


Figure 2.3 Crane Loading Conditions (MBMA 2012).

1.2 Connection Detail

According to Ting, Shanmugam et al. (1991), beam-to-column connections in steel frames can be classified into three categories, ~ viz. types 1, 2 and 3. A type 1 is called a rigid connection that connection is assumed to be capable of transferring the full moment. This type of connection will result in a more economical beam design, but the column will have to be checked for the extra moment imposed. A type 2 connection is the simple connection where no moment is transferred between the beam and the column. A type 3 connection, also known as a semi-rigid connection, transfers only a portion of the moment between the beam and the column.

Nowadays, there has been enlarged use of hollow structural sections (HSS) in recent years. In particular, HSS are predominantly available in three shapes: rectangular hollow sections (RHS), square hollow sections (SHS), and circular hollow sections (CHS). Moment connections in tubular structures have many features and can be shown in Figure 2.4.

column/chord	beam/brace	designation
○	○	CC
○	□	RC
○	I	IC
□	□	RR
□	○	CR
□	I	IR
I	○	CI
I	□	RI

Figure 2.4 Designation of moment connections with hollow section members
(Kurobane 2004).

According to Wardenier, Packer et al. (2002), connection between corbels and hollow sections is similar to I beam attached with column in T-joint connection. Beam-to-column connections can be welded or bolted. This thesis will focus mainly on unstiffened welded connections between CHS or SHS columns and I-section beams, as shown in Figure 2.5.

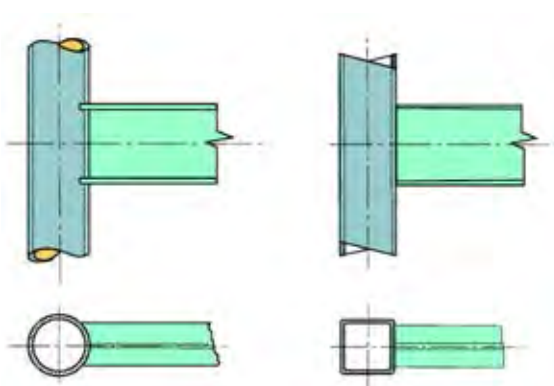


Figure 2.5 Unstiffened I-beam-to-CHS or SHS connections (Wardenier, Packer et al. 2002).

1.3 Beam to column connection

1.3.1 Introduction

From the sixties to the eighties, expansive experimental researches had been performed on different types of connections using rectangular hollow steel section (RHS) members. The studies had been primarily focused on welded uniplanar connections where RHS was used both for chord and braced member, such as X-, T, and K-joints in RHS. Those connections had been tested with axial loading, in-plane bending and out-of-plane bending moments. The experimental and analytical work regarding weld connections in structural hollow sections before 1982 had been summarized by Wardenier (1982).

1.3.2 I-beam to RHS column connections

In 1981, a total of 10 uniplanar I-beam to RHS column T-joints loaded by in-plane bending moments had been tested in Kanatani, Fujiwara et al. (1981). The test results provided useful information on the behavior of unstiffened RHS moment connections. Kanatani indicated that generally four local failure modes, i.e. chord face yielding, chord side wall failure, local buckling of brace flanges and punching shear, can be expected for this type of connection. The connection strengths of the Japanese tests are summarized in Table 1. Some of the results deviate somewhat from those given in Kanatani, Fujiwara et al. (1981) due to the fact that peak loads were used.

Table 1 Summary of the test results for I-beam to RHS connections (Kanatani, Fujiwara et al. 1981).

Test specimens	Chord $b_0 \times h_0 \times t_0$ (mm)	I-beam $h_1 \times b_1 \times t_w \times t_1$ (mm)	β	2γ	f_{y0} (N/mm ²)	$M_{u,exp}$ (KNm)
H1	200x200x6	148x100x6x9	0.50	33.3	383	8.4
H2		300x150x6.5x9	0.75			42.2

H3		300x200x6x9	1.00			91.6
H4		400x200x8x13	1.00			106.7
H5	200x200x9	148x100x6x9	0.500	22.2	340	19.5
H6		300x150x6.5x9	0.75			76.0
H7		300x200x6x9	1.00			137.7
H8	200x200x12	148x100x6x9	0.50	16.7	378	31.8
H9		300x150x6.5x9	0.75			122.7
H10		300x200x6x9	1.00			187.0

Where β is chord-width ratio (b_1/b_0), 2γ is width to thickness ratio of the column (b_0/t_0), f_{y0} is yield stress of the columns and $M_{u,exp}$ is experimentally determined ultimate strength for connection loaded by in-plane bending moments.

2. Von-Mises Stress

2.1 Definition of Yield strength

Yield strength or yield stress is the material property defined as the stress at which a material begins to deform plastically whereas yield point is the point where nonlinear (elastic + plastic) deformation begins. Before stress goes to the yield point, the material will deform elastically and will return to its original shape when the applied stress was removed that is elastic behavior. Once the stress reaches the yield point and passed, the material will deform permanently and non-reversible to its original shape we call as a plastic or inelastic behavior. Figure 2.6 illustrated the components of stress and strain curve.



1413517646

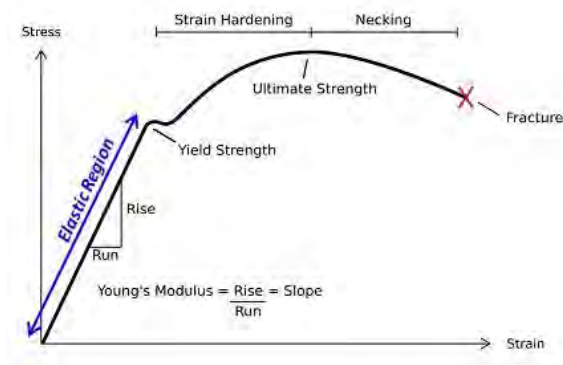
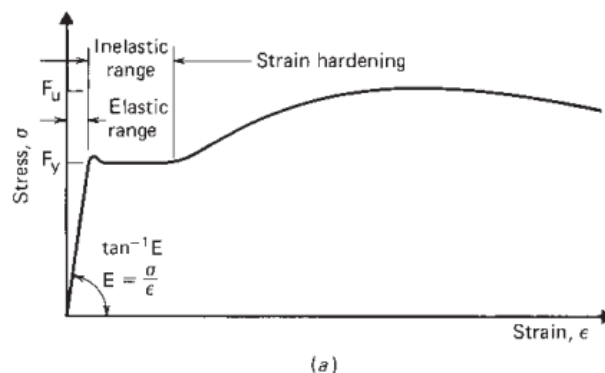


Figure 2.6 Stress-Strain Curve.

Failure of engineering materials can be classified into ductile and brittle failure. In reality, most of the metals are ductile and fail due to yielding. The yield strength can characterize their failure also. For example, ceramics and glasses are brittle and fracture or rupture when the stress exceeds the yield point a bit. Their behaviors of stress and strain are linear up to the point of failure and they fail instantly.

In the 2007 edition of the North American Specification, the generic term yield stress is used to denote either yield point or yield strength, the yield stresses of steels listed in the North American specification range from 165-552 MPa. There are two general types of stress-strain curves as shown in Figure 2.7. One is of sharp-yielding type and the other is of gradual-yielding type.



(a)

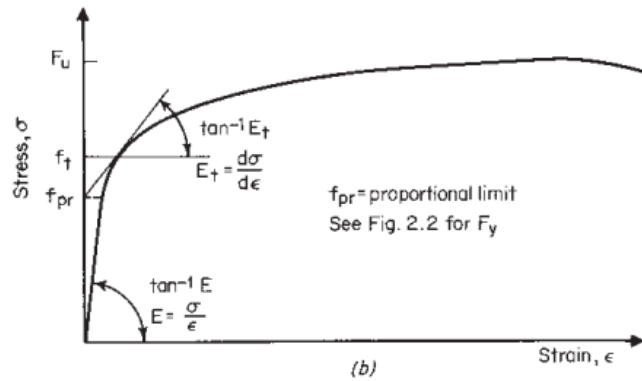


Figure 2.7 Stress–strain curves of carbon steel sheet or strip: (a) sharp-yielding for hot-rolled; (b) gradual yielding for cold-formed (Yu 2000).

2.2 Index Notations

According to Jones (2009), the mechanic continuum have general notion of stress that was create by Cauchy , we called as a Cauchy stress tensor σ_{ij} or simply call as a stress tensor as shown in Figure 2.8. In three dimension of infinitesimal body, state of stress be given by the three normal stresses $\sigma_{xx}, \sigma_{yy}, \sigma_{zz}$ and tangential stresses (shearing stress) $\tau_{xy}, \tau_{xz}, \tau_{yz}$. That can be represented in matrix as

$$\begin{bmatrix} \sigma_{xx} & \tau_{xy} & \tau_{xz} \\ \tau_{yx} & \sigma_{yy} & \tau_{yz} \\ \tau_{zx} & \tau_{zy} & \sigma_{zz} \end{bmatrix}$$

We already known that in the matrix form of stress tensors, the stress must be symmetry to satisfy the equilibrium condition that is, $\tau_{xy} = \tau_{yx}$ $\tau_{xz} = \tau_{zx}$ and $\tau_{yz} = \tau_{zy}$.

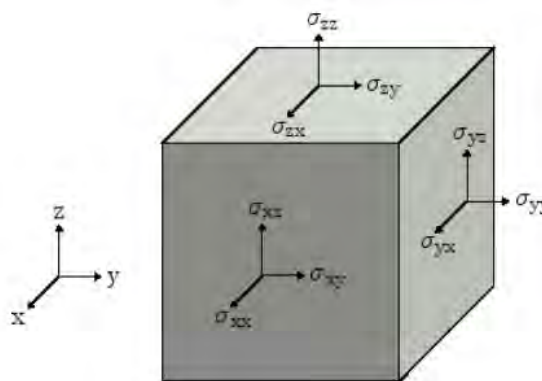


Figure 2.8 Stress components acting on infinitesimal cube.

2.3 Maximum Distortion Energy Theory (von Mises yield criterion)

This criterion is based on the determination of distortion energy in given material of the energy associated with change in the shape of that material. The von Mises yield criterion can be also formulated in terms of the von Mises stress or equivalent tensile stress σ_v . The von Mises stress is a scalar value that can be computed from the Cauchy stress tensor that already described in section 2.2. According to this theory, a given structure will be safe as long as von Mises stress is still less than the yield strength, σ_y . The properties of von Mises stress is used to predict yielding of material under complex loading from the result of uniaxial tensile tests. According to Von Mises (1913), the yield criterion can be written in term of stress components in general form as

$$\sigma_v = \sqrt{\frac{(\sigma_{xx} - \sigma_{yy})^2 + (\sigma_{yy} - \sigma_{zz})^2 + (\sigma_{zz} - \sigma_{xx})^2 + 6(\tau_{xy}^2 + \tau_{yz}^2 + \tau_{xz}^2)}{2}}$$

In three-dimensional solid mechanic, the general form of von-Mises stress can be reduced and written in term of principal stress as

$$\sigma_v = \sqrt{\frac{(\sigma_1 - \sigma_2)^2 + (\sigma_2 - \sigma_3)^2 + (\sigma_3 - \sigma_1)^2}{2}}$$

This equation can be represented as a cylindrical to define the yield surface that displayed in Figure 2.9. That is a circle with radius $\sqrt{2}\tau$ when τ is a yield stress of the material under pure shear loading, i.e., $\sigma_1 = -\sigma_2 = \tau$. The magnitude of yield stress in pure shear, τ is $\frac{\sigma_y}{\sqrt{3}}$ that shown in Figure 2.10.



1413517646

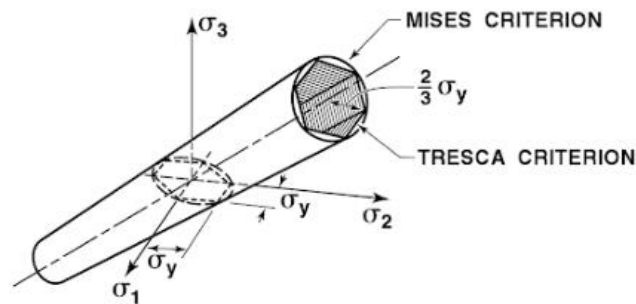


Figure 2.9 Mises versus Tresca yield surfaces (Jones 2009).

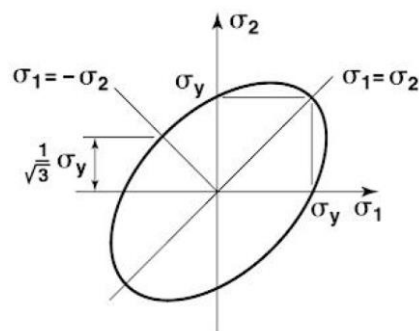


Figure 2.10 Mises yield criterion for biaxial stresses (Jones 2009).

3. Finite element.

3.1 Introduction

Finite element methods are a computer-based numerical technique, and can be used to calculate deflection, stress, vibration, buckling and many other phenomena of many structural engineering problems. The methods can also be used to analyses either small or large-scale deflection under loading or applied displacement; and can reduce costs in physical tests. Thus, finite element methods have been extensively used in steel structure analyses. In the finite element method, a structure is divided into many small simple blocks or elements (finite element discretization). The behavior of an individual element can be described with a relatively simple set of equations. The equations, describing individual element behavior, are joined into a large set of equations that describe the behavior of the whole structure. The computer can solve this large set of simultaneous equations. From the solution, the computer extracts the behavior of individual elements, and

obtains the stress and deflection of every part of the structure. The stresses will be compared to the allowed value of stress for materials to be used, to check if the structure is sufficiently strong. However, the most difficult part of finite element analyses from the practice point of view is to develop an accurate model which can correctly represent the whole structural system. Thus, the creation of a reliable finite element model is a primary aim for any structure analysis (Wu 2013).

3.2 SOLID185 Homogeneous Structural Solid Element Description.

Finite element commercial software (ANSYS) was provided SOLID185 as a three dimensional solid element. This element can be used to modeling many 3-D solid structures. From Figure 2.11 illustrated the infinitesimal element that defined by eight nodes and the isotropic material properties. Each node have three degree of freedom ,viz., translations in the nodal x, y and z directions. The general coordinate system in this element is along global directions.

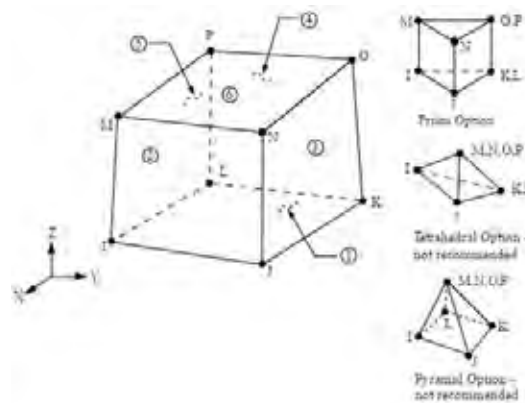


Figure 2.11 Finite Element SOLID185 geometry (ANSYS 2017).

4. Cold-Formed Structural Steels.

4.1 General Remark

In steel construction market, we can separate the steel member into two types. The first type includes hot-rolled shapes and members built-up of plates while the second type includes cold-formed members obtained from roll forming. The used in cold-formed steel structural members ranges from 0.4mm to 6.4mm,

The mass-produced cold-formed products have yielding stresses within the range of 250 to 600 MPa, ultimate stresses within the range of 300 to 720 MPa (Henriques De Sena Cardoso 2015).

The main differences between hot-rolled sections and cold-formed sections are shown below (Yu 2000, Henriques De Sena Cardoso 2015).

- (1) Both of them have the same materials and processing time, in which cold-formed section is a kind of economical steel, the weight of cold formed is relatively light.
- (2) High slenderness values for the cross-section walls (ratio width/thickness), the cold-formed allows local buckling, which can make full use of bending bearing capacity. While, hot-rolled steel does not allow local buckling.
- (3) The free torsional rigidity of hot-rolled steel is higher than that of cold formed.
- (4) Hot-rolled sections have smaller corner radii, they generally also have a larger cross-sectional area than cold formed hollow sections. This advantages become more significantly with greater wall thicknesses.
- (5) Cold formed sections have greater brittleness in the corner. The tensile test is used to measure ductility using specimens in a longitudinal direction, in cold formed sections, ductility is essentially reduced, the below graph Figure 2.12 that indicating differences in ductility.

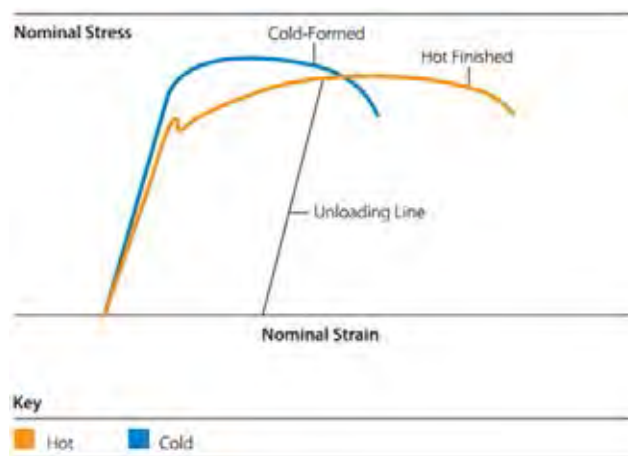


Figure 2.12 The relationship between strain and stress of cold-formed and hot-rolled sections.

(6) Comparing the buckling loads on 3m columns of hot-rolled and cold formed hollow sections that are subjected to the same 500kN axial compression. The diagrams in Figure 2.13 illustrate that cold-formed sections will save more material than hot-rolled sections.

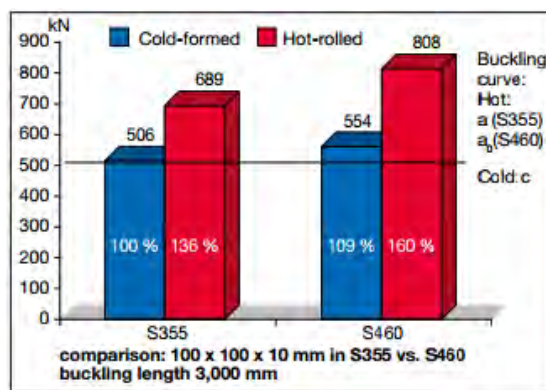


Figure 2.13 The practical effects by comparing the buckling loads on columns of hot-rolled and cold-formed hollow sections.

Therefore, the analysis and design of cold-formed steel structures is more demanding than other structural elements and the main complexity is associated with the buckling behavior.

4.2 Local Buckling of Columns.

All column section consisted of plate elements. These plate elements can buckle locally before the overall buckling of the column occurs. Local buckling is an extremely important facet of cold formed steel sections on account of the fact that the very thin elements used will invariably buckle before yielding.

Figure 2.14 illustrated plate with high value of width to thickness ratio (b/t) will buckle under lower critical stress than plates with low b/t value. However, it can carry more load and reached the maximum load in the post-buckling strength region. Plate with high b/t value will have larger reserved strength than the plate with low b/t .

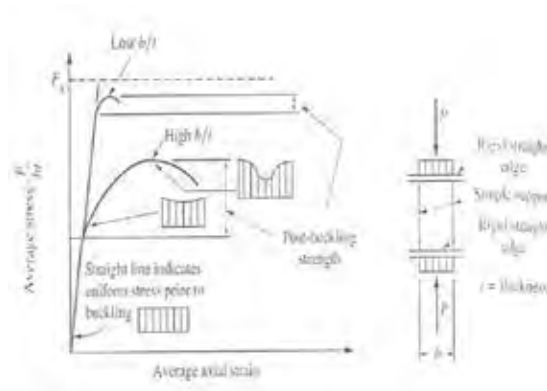


Figure 2.14 Comparison of Plate strength and various b/t ratios (Thepchatri 2017).

4.3 Inelastic Buckling Analysis

According to Mangat (1969), after solving differential equation by using Laplace’s operator. The general equation for local buckling is

$$f_{cr} = \frac{k\pi^2 E}{12(1-\mu^2)(b/t)^2}$$

where $k = \left(\frac{mb}{a} + \frac{a}{mb}\right)^2$ that is plate buckling coefficient, a and b are length and width of plate respectively and m is a number of half sine wave in the x axis. Plots of k with a/b with various values of m are displayed graphically in Figure 2.15. It is noted that for simple support (S.S.) plate the k has the minimum value of 4 for all cases.

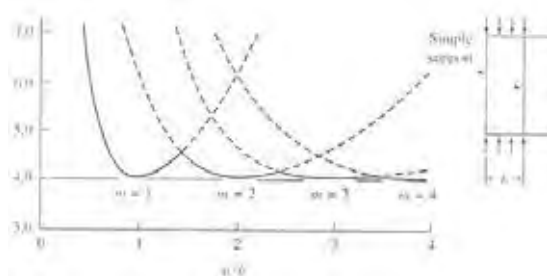


Figure 2.15 Graph of k vs a/b with various m values (Thepchatri 2017)

The k values for different plate boundary conditions are depicted in Figure 2.16. It clearly shown that the boundary conditions along the loaded edges do not

change the k value from simply support case. The above equation is for the elastic local buckling stress, for inelastic range we get

$$f_{cr,in} = \frac{k\pi^2 E \sqrt{\tau}}{12(1-\mu^2)(b/t)^2}$$

where $\tau = E_t / E$, E_t is a tangent modulus of elasticity and E is Young's modulus.

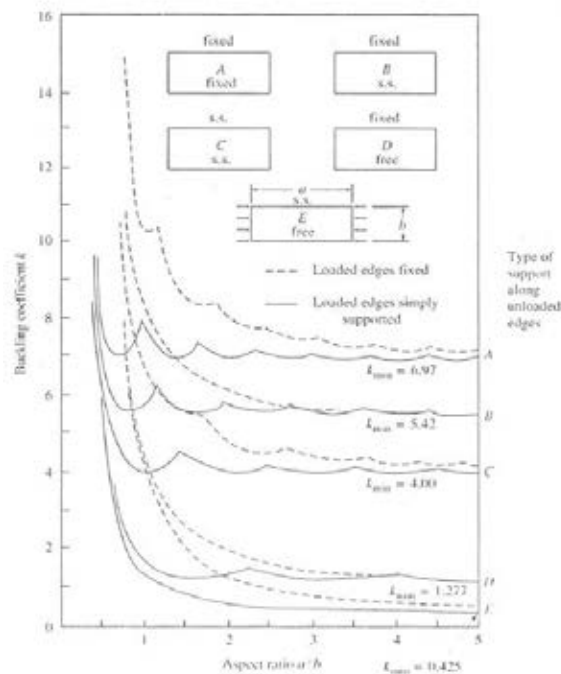


Figure 2.16 k values for different plate boundary conditions.

4.4 Design Concept of Structural Steel Members.

(1) The design flexural strength for box section

AISC 360-16 (2016) classified compression elements members subject to flexure in to 3 categories are. compact section ($\lambda \leq \lambda_p$), noncompact section ($\lambda_p < \lambda \leq \lambda_r$) and slender section ($\lambda > \lambda_r$) when λ need to considered separately in flanges λ_f and webs λ_w element. For flanges element $\lambda_{pf} = 1.12\sqrt{E/F_y}$ and $\lambda_{rf} = 1.40\sqrt{E/F_y}$. For webs element $\lambda_{pw} = 2.42\sqrt{E/F_y}$ and $\lambda_{rw} = 5.70\sqrt{E/F_y}$.

From AISC (2016) The nominal flexural strength, M_n shall be the lowest value obtained from Eq.(1), Eq.(2), Eq.(3) and Eq.(5) according to the limit states of yielding (plastic moment), flange local buckling, web local buckling under pure flexure.

For compact section the moment capacity is equal to plastic moment of the section

$$M_n = M_p = F_y Z \quad (1)$$

For section with noncompact flange nominal moment capacity is

$$M_n = M_p - (M_p - F_y S) \left(3.57 \frac{b}{t_f} \sqrt{\frac{F_y}{E}} - 4.0 \right) \quad (2)$$

For section with slender flange nominal moment capacity is

$$M_n = F_y S_e \quad (3)$$

where Z is plastic section modulus about the axis of bending, S is elastic section modulus about the axis of bending and S_e is effective section modulus determined with the effective width. The effective width, b_e is determined as Eq. (4).

$$b_e = 1.92 t_f \sqrt{\frac{E}{F_y}} \left(1 - \frac{0.38}{b/t_f} \sqrt{\frac{E}{F_y}} \right) \quad (4)$$

For section with noncompact webs nominal moment capacity is

$$M_n = M_p - (M_p - F_y S) \left(0.305 \frac{h}{t_w} \sqrt{\frac{F_y}{E}} - 0.738 \right) \quad (5)$$

Where h is depth of web and t_w is thickness of web. There are no HSS for section with slender webs.

(2) The design compressive strength for SHS.

According to AISC 360-16 (2016), the specification classified compression elements members subject to axial compression in to 2 categories viz. non-slender element section ($\lambda \leq \lambda_r$) and slender element ($\lambda > \lambda_r$) when λ is width to-thickness

ratios of compression elements (b/t) and $\lambda_r = 1.4\sqrt{E/f_y}$. The nominal compressive strength for non-slender element compression members, P_n shall be determined based on Eq. (6)

$$P_n = F_{cr}A_g \quad (6)$$

The critical strength, F_{cr} is determined as follows

when $F_y / F_e \leq 2.25$

$$F_{cr} = F_y(0.658^{F_y/F_e}) \quad (7)$$

when $F_y / F_e > 2.25$

$$F_{cr} = 0.877F_e \quad (8)$$

where F_e elastic buckling stress determined according to Eq.(9).

$$F_e = \pi^2 E / (L_c / r)^2 \quad (9)$$

where L_c is effective length of member (KL) and r is radius of gyration.

The nominal compressive strength for slender-element compression members shall be determined with Eq. (10)

$$P_n = F_{cr}A_e \quad (10)$$

where A_e is summation of the effective areas of the cross section based on reduced effective widths. The effective width, b_e for slender elements is determined as Eq.(11) and Eq. (12)

when $\lambda \leq \lambda_r \sqrt{\frac{F_y}{F_{cr}}}$

$$b_e = b \quad (11)$$

when $\lambda > \lambda_r \sqrt{\frac{F_y}{F_{cr}}}$

$$b_e = b \left(1 - c_1 \sqrt{\frac{F_{el}}{F_{cr}}} \right) \sqrt{\frac{F_{el}}{F_{cr}}} \quad (12)$$

where b is width of the element, c_1 is effective width imperfection adjustment factor equal to 0.2 for square and rectangular HSS, c_2 is equal to 1.38 for square HSS and F_{el} is elastic local buckling stress determined by $\left(c_2 \frac{\lambda_r}{\lambda} \right)^2 F_y$.

(3) The design specification for combine axial force and bending moment.

AISC 360-16 (2016) provided load combination under compression and flexure force in doubly symmetric members shall be limited by Eq. (13) and Eq. (14)

when $\frac{P_r}{P_c} \geq 0.2$

$$\frac{P_r}{P_c} + \frac{8}{9} \left(\frac{M_{rx}}{M_{cx}} + \frac{M_{ry}}{M_{cy}} \right) \leq 1.0 \quad (13)$$

when $\frac{P_r}{P_c} < 0.2$

$$\frac{P_r}{2P_c} + \left(\frac{M_{rx}}{M_{cx}} + \frac{M_{ry}}{M_{cy}} \right) \leq 1.0 \quad (14)$$

For allowable strength design method (ASD)

where P_r is required axial strength of columns, P_c is available axial strength of columns (P_n / Ω_c), M_r is required flexural strength of columns, M_c is available flexural strength of columns (M_n / Ω_b), Ω_c is safety factor for compression equal to 1.67, Ω_b is safety factor for flexure equal to 1.67, x is subscript relating symbol to major axis bending and y is subscript relating symbol to minor axis bending.

Term on the left-hand side from Eq. (13) and Eq. (14) called as stress ratio. The column can be resisted the load if stress ratio is less than 1. The load collapse from specification code can be determined from Eq. (15).

$$\alpha_{AISC} = \frac{1}{SR} \quad (15)$$

where α_{AISC} is load collapse or safety factor in an engineering sense from specification code and SR is Term on the left hand side from Eq. (13) and Eq. (14).

4.5 Column plastification.

The plastification of the I-beam to RHS column connection is not only determined by the connection of the flanges but also by the column depth. In general, the plastic failure of a steel HSS column connected to corbel loaded in-plane bending moments can be classified in to 2 categories. The first one is chord face yielding behavior. Another failure behavior of the I-beam to RHS column connection is chord side wall failure.

4.5.1 Chord face yielding

For chord face yielding failure, a simplified analytical yield line model is display in Figure 2.17. Lu (1997) provided the ultimate moment strength formulae describing the chord face yielding behavior by Eq. (16)

$$M_{1,u,xb} = (0.5 + 0.7\beta) \frac{4}{\sqrt{1 - 0.9\beta}} f_{y0} t_0^2 h_m \quad (16)$$

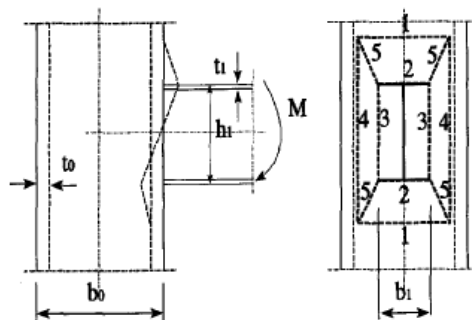


Figure 2.17 Chord face yield line model (Lu 1997).

4.5.2 Chord side wall failure

According to Lu (1997), for $\beta=1$, the connection strength can be based on chord side wall failure. The analytical model for chord side wall failure and strength formulae are shown in Figure 2.18, Eq. (17) and Eq. (18).

$$M_{1,u,xb} = 2(t_1 + 5t_0) f_{y0} t_0 (h_1 - t_1) \quad \text{for} \quad h_1 \geq 2t_1 + 5t_0 \quad (17)$$

$$M_{1,u,xb} = 0.5(h_1 + 5t_0)^2 f_{y0} t_0 \quad \text{for} \quad h_1 < 2t_1 + 5t_0 \quad (18)$$

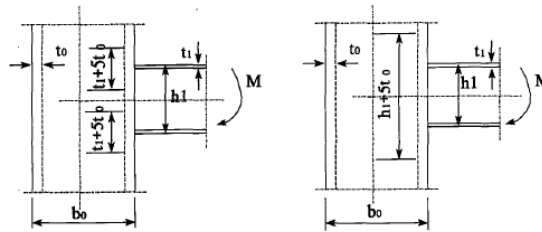


Figure 2.18 Chord side wall failure (Lu 1997).

where β is the ratio of overall branch width to chord width for square HSS (b_1/b_0), b_1 is width of overall branch, b_0 is width of the square HSS column, f_{y0} is yield stress of the square HSS member, t_0 is wall thickness of the square HSS column, h_m is $h_1 - t_1$, h_1 is depth of a branch member and t_1 is thickness of the flange of a branch member

The load collapse from Lu (α_{ref}) can be determined from Eq. (15) by substituting M_n into $M_{1,u,xb}$, where the stress ratio is computed in Eq. (13) or (14).

5. Non-linear analysis for estimating limit loads.

5.1 Arc-length method

5.1.1 Introduction.

Riks (1979) provided an incremental approach to the solution of buckling and snapping problems called arc-length method. The arc-length method is suitable for nonlinear static equilibrium solutions of unstable problems. A structure can become unstable when a load reaches its buckling value or when nonlinear material becomes unstable. Application of the arc-length method involves the tracing of a complex path in the load-displacement response into the buckling and post buckling

regimes. It is assumed that all load magnitudes can be controlled by a single scalar parameter called load factor.

5.1.2 General Equation.

Mathematically, the arc-length method can be viewed as the trace of a single equilibrium curve in a space spanned by the nodal displacement variables and the total load factor. The arc-length method itself is an automatic load step method. In the arc-length procedure, general equation is described in Eq. (19)

$$\left[K_i^T \right] \{ \Delta u_i \} = \lambda \{ F^a \} - \{ F_i^{nr} \} \quad (19)$$

where $\left[K_i^T \right]$ is jacobian matrix, i is subscript representing the current equilibrium iteration, $\{ F^a \}$ is vector of applied loads, $\{ F_i^{nr} \}$ is vector of restoring loads corresponding to the element internal loads, $\{ u_i \}$ vector of unknown DOF (degree of freedom) values and λ is the total load factor. The Arc-length approach with full Newton-Raphson method is depicted graphically in Figure 2.19. The loading factor can be written in an incremental form at substep n and iteration i as shown in Eq.(20).

$$\left[K_i^T \right] \{ \Delta u_i \} - \Delta \lambda \{ F^a \} = (\lambda_n + \lambda_i) \{ F^a \} - \{ F_i^{nr} \} = - \{ R_i \} \quad (20)$$

where $\{ R_i \}$ is the residual vector, the incremental displacement $\{ \Delta u_i \}$ can be expressed into two parts

$$\{ \Delta u_i \} = \Delta \lambda \{ \Delta u_i^I \} + \{ \Delta u_i^{II} \} \quad (21)$$

where

$$\{ \Delta u_i^I \} = \left[K_i^T \right]^{-1} \{ F^a \} \quad (22)$$

$$\{ \Delta u_i^{II} \} = - \left[K_i^T \right]^{-1} \{ R_i \} \quad (23)$$

We can define one vector between the previous equilibrium point and a point determined in iteration i by

$$t_i = \{ \Delta u_n \} + \psi \lambda_i \quad (24)$$



1413517646

CD IThesis 6070287021 thesis / rev: 01082562 19:12:57 / seq: 13

where $\{\Delta u_n\}$ is the incremental accumulated displacement over the current time step and ψ is the scaling vector for unit displacement. The norm of this vector is

$$|t_i| = \sqrt{\{\Delta u_n\}^t \{\Delta u_n\} + \psi^2 \lambda_i^2} \quad (25)$$

when iteration $i+1$, the vector in Eq. (25) becomes

$$t_{i+1} = \{\Delta u_n\} + \{\Delta u_i\} + \psi(\lambda_i + \Delta\lambda) \quad (26)$$

According to Crisfield (1981), assumes that norm of the vector is constant along the equilibrium in each iterations, that is

$$|t_i| = |t_{i+1}| \quad (27)$$

Using Eq. (21) and substituting by Eq. (24) and Eq. (26), the following quadratic equation becomes

$$a(\Delta\lambda)^2 + b(\Delta\lambda) + c = 0 \quad (28)$$

where

$$a = \psi^2 + \{\Delta u_i^I\}^t \{\Delta u_i^I\} \quad (29)$$

$$b = 2\left(\psi^2 \lambda_i + \{\Delta u_n\}^t \{\Delta u_i^I\} + \{\Delta u_i^{II}\}^t \{\Delta u_i^I\}\right) \quad (30)$$

$$c = 2\{\Delta u_n\}^t \{\Delta u_i^{II}\} + \{\Delta u_i^{II}\}^t \{\Delta u_i^{II}\} \quad (31)$$

This quadratic equation system has two real roots, $\Delta\lambda^{(1)}$ and $\Delta\lambda^{(2)}$, which both satisfy the constant arc-length radius. For each of these roots, the angle between vector t_{n-1} in the previously converged substep, and vector t_{i+1} in the current substep. This angle can be obtained from Eq. (32).

$$\cos(\theta) = \frac{(t_{i+1})^T \cdot (t_{n-1})}{|t_n| \cdot |t_{n-1}|} \quad (32)$$

To move the equilibrium path forward, the route for which the cosine of the associated angle should be close to 1. Finally, the solution vectors are updated according to

$$\{\Delta u_{i+1}\} = \{u_n\} + \{\Delta u_n\} + \{\Delta u_i\} \quad (33)$$

And

$$\lambda_{i+1} = \lambda_n + \lambda_i + \Delta \lambda \quad (34)$$

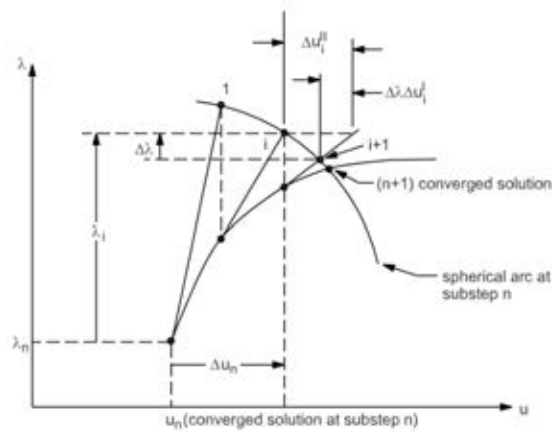


Figure 2.19 Arc-Length Approach with Full Newton-Raphson Method.

6. Stiffened Tubular T-joint connection.

6.1 Introduction.

According to Voth and Packer (2012), thin walled tubular connections is often required that the region around the connection be stiffened to limit chord plastification or excessive deformation. The way to stiffening schemes have been developed including internal stiffening of the chord or using the steel plate to attach around the beam-column connection called external ring stiffener. There are still have a lot of method to stiffening the connection between chord and brace. The main propose of this idea is to enhance the strength of the column for carrying the intensive load.

6.2 Internal plate strengthening technique.

Nowadays, internal annular ring stiffened connection have been used in both onshore and offshore structures as a method to prevent against premature local buckling failures and chord plastification.

Lee and Llewelyn-Parry (1999) performed non-linear finite element of T-joint connection between CHS column and CHS beam under axial compression load. The boundary support condition of the model displayed in Figure 2.20. Geometry and detail of internal annular ring stiffened displayed in Figure 2.21. The use of internally stiffened joints to enhance static capacity and to reduce stress concentration was common practice in the design of fixed steel platforms. The study shows that internal ring stiffener can significantly improve strength of the column. The thickness and depth of web in stiffener has affected to the strength of column. The result of strength capacity displayed graphically in Figure 2.22.

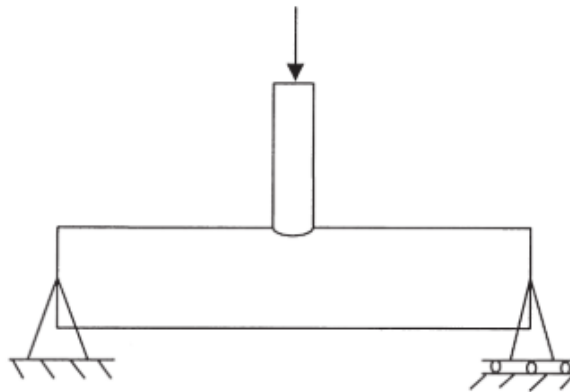


Figure 2.20 Boundary support conditions (Lee and Llewelyn-Parry 1999)

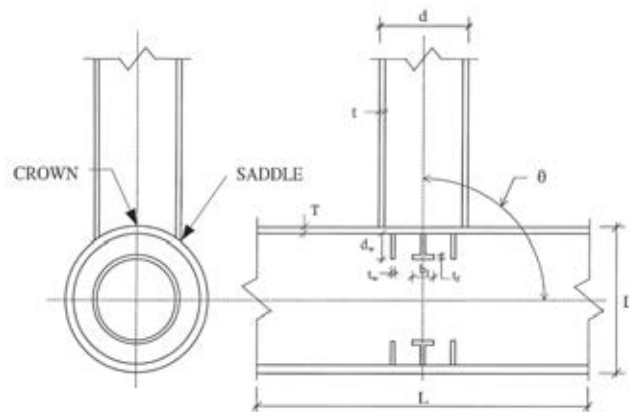


Figure 2.21 Internal annular ring stiffened (Lee and Llewelyn-Parry 1999)

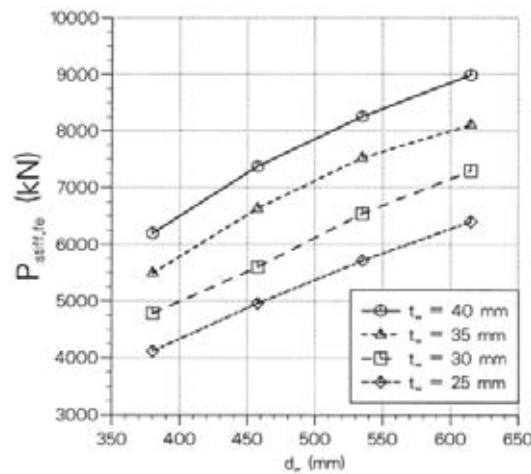


Figure 2.22 Relationship between stiffener strength and d_w for different t_w (Lee and Llewelyn-Parry 1999)

Lee and Llewelyn-Parry (2004) presented the numerical study on the strength of tubular T-joints with centrally located plain annular ring stiffeners under brace compression loading. The study shows that stiffeners positioned at the saddle position provide a better strength enhancement than those at the crown positions.

Ahmadi, Lotfollahi-Yaghin et al. (2012) performed the finite element analysis to study the effect of geometrical parameters on the chord-side stress concentration factors between the outer (inclined) brace and the chord in internally ring-stiffened tubular KT-joints subjected to balanced axial loads. The geometrical details of the internally ring-stiffened specimen are displayed in Figure 2.23. The boundary

condition is both chord ends were assumed to be fixed, displacements of the nodes on the symmetry plane were restrained perpendicular to the plane and the static loading applied at the end of the central (vertical) brace. The result show that chord-side stress concentration factors along the weld toe of the intersection between the outer brace and the chord was reduced when applied the internal ring stiffener to the model.

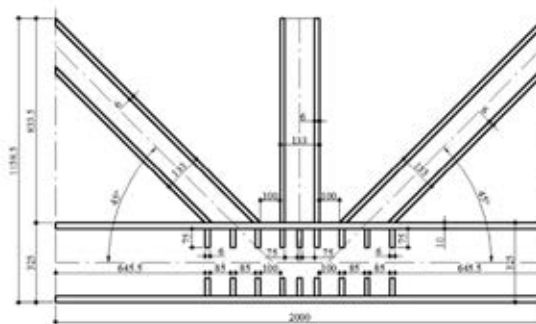


Figure 2.23 Geometrical details of the internally ring-stiffened KT-joint specimen (Ahmadi, Lotfollahi-Yaghin et al. 2012).

6.3 External ring strengthening technique.

The external ring stiffened connection or through-diaphragm connection is modern and popular technique for enhance maximum load capacity of the column to prevent against premature local buckling failures and chord plastification. Some of the literature reviews are generated the idea to provide this strengthening technique.

Wu (2013) study numerical model of RHS column to I-beam connection. The connection panel is actually a stub-column groove welded to the through diaphragms at the ends. The geometrical details of the connection and fabrication of the bottom-through-diaphragm are depicted in Figure 2.24 and Figure 2.25. The study shows that the plastic hinge away from the column face. This type of connection may be avoided premature occurrence of brittle fractures.

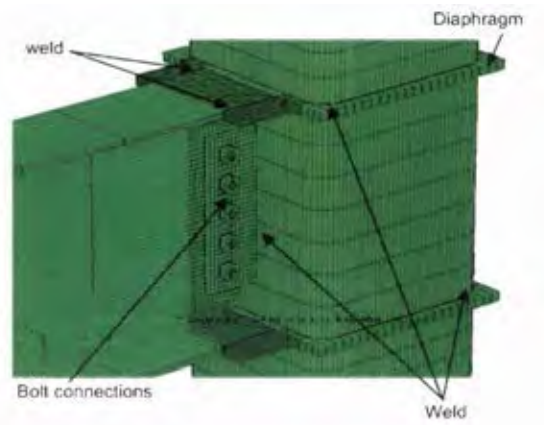


Figure 2.24 Column, beam, diaphragm and fin plate (Wu 2013).

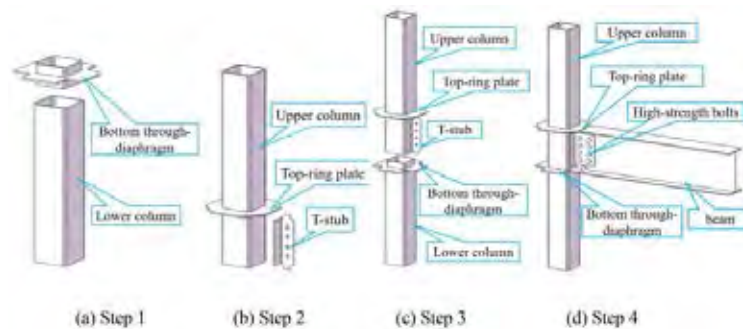


Figure 2.25 Fabrication of the bottom-through-diaphragm and top-ring connection (Cao, Shu et al. 2018).

T. Uraipong (2016) study the strength enhancement of the connection between I-beam and the circular hollow section column. The strengthening technique using steel plate installed horizontally around the column. The geometry of steel plate covered the circular hollow section column displayed in Figure 2.26. The result clearly shows that when increase the width of stiffener plate will improve strength of the connection approximately 20 to 40 percent.

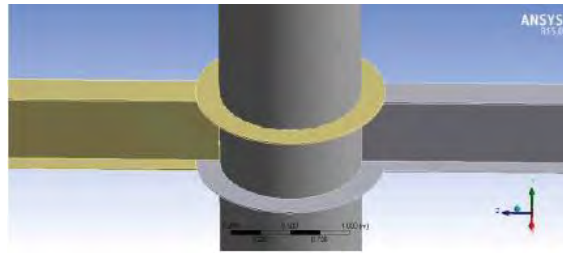


Figure 2.26 Geometrical detail of steel plate installed horizontally around the column (T. Uraipong 2016)



1413517646

CU IThesis 6070287021 thesis / recv: 01082562 19:12:57 / seq: 13

CHAPTER 3 METHODOLOGY.

1 Finite Element Modelling of Column and Connection Structures.

1.1 Material properties

In this thesis, A standard steel profiles in the company are using for the structure purposes in construction and for pipeline systems. For the finite element analysis, material of column will be SS400 steel structure with yield stress equal to 235 MPa. Material for beam connection will be A36 steel structure. Since we consider only the capacity for a column, yield strength for beam connection will not applied in the model. The modulus of elasticity and Poisson's ratio for both materials are 200000 MPa and 0.3. To performed non-linear with plastic analysis, material property in the column that modeling in this thesis is elastic perfectly plastic with tangent modulus for all materials are equal to zero.

1.2 Geometry

Eight steel hollow steel section columns detailed in Table 2 were considered to illustrate applications of the proposed scheme. A catalog with using cold-formed steel hollow sections, namely square hollow steel (SHS), the analyses considered for various thicknesses ranging from 5 to 12 millimeter. The two standard steel corbels (namely H-250x250x11x11 and H-300x300x10x15) were employed, where the corbel with 250 mm width connected to the steel HSS column with 250 mm width and ones with 300 mm width to the column of 300 mm width. The contact location was 30 cm offset to the column face. Since column and corbel are the same width, the geometry brace to chord width ratio β will equal to 1 as shown in Figure 3.1. Shape of geometry are already shown in Figure 2.5.



1413517646

CD :Thesis 6070287021 thesis / rev: 01082562 19:12:57 / seq: 13

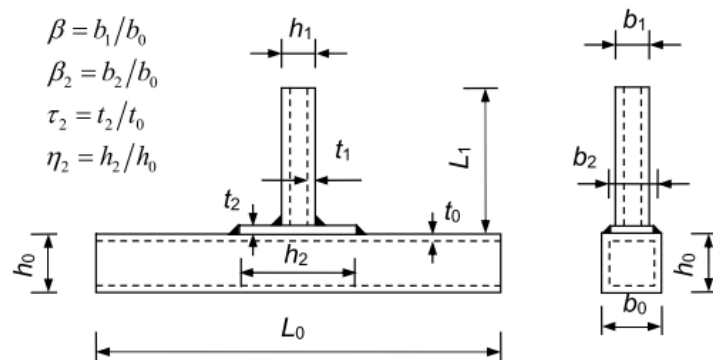


Figure 3.1 T-joint Connection design model (Chang, Xia et al. 2014).

Table 2 Geometry of steel HSS columns.

Example	Chord Width (mm)	Chord Thickness (mm)
1	250	5
2	250	6
3	250	8
4	250	9
5	250	12
6	300	6
7	300	9
8	300	12

1.3 Finite Element Types and Discrete Structural Model

The responses of steel HSS columns under crane loads were mapped out using the nonlinear 3D FE analyses. The columns were modeled using a series of eight-node solid FEs within the commercial ANSYS software. The element type namely SOLID185 for the columns and corbels are used in this thesis. Since the column and corbels are different material, the model will have 2 element types and 2 material models that depicted in Figure 3.2. The columns are nonlinearity material properties, bi-linear isotropic hardening plasticity with tangent modulus equal to zero was applied in the model. The uniform 10 mm-size mesh construction was adopted for the column having 1 m in length.

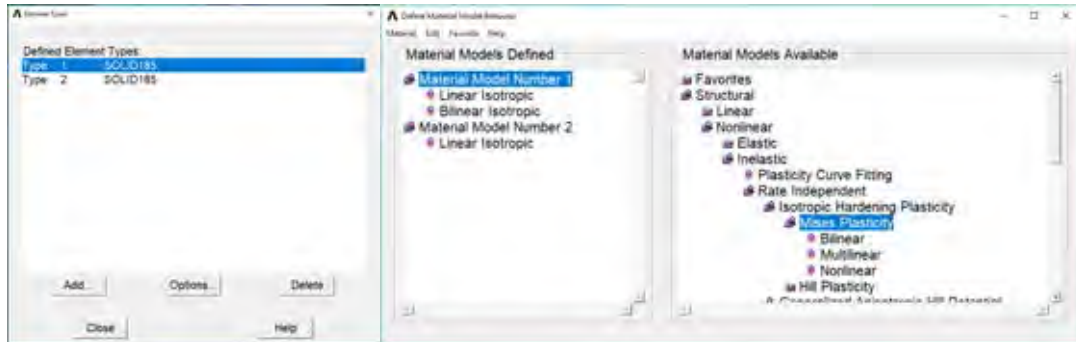


Figure 3.2 Element types and Material model in the project.

1.4 Load and Boundary Conditions

(1.) Crane loads computation

This thesis considers only the maximum vertical crane load which came from maximum wheel loads. The maximum wheel loads can be computed as

$$WL = \frac{RC + HT + 0.5CW}{NW_b}$$

From the catalog with crane capacity equal to 20 US tons, the detail shown that crane capacity equal to 177.9 KN. Bridge weight and trolley with hoist weight are equal to 12701 kg and 2767 kg respectively. Since number of end truck wheels at one end of the bridge are equal to 2, the maximum wheel loads can be computed as

$$WL = \frac{177.9 + 27.67 + 0.5 \times 127.01}{2} = 134.5375 \text{ KN}$$

Each side of end truck have 2 wheels, the maximum wheel loads need to multiply by 2 that is become approximately 270 KN. The crane load was uniformly applied to over the contact area of corbel from end of the brace to 20 cm offset. Loading condition detail in the model depicted in Figure 3.3.

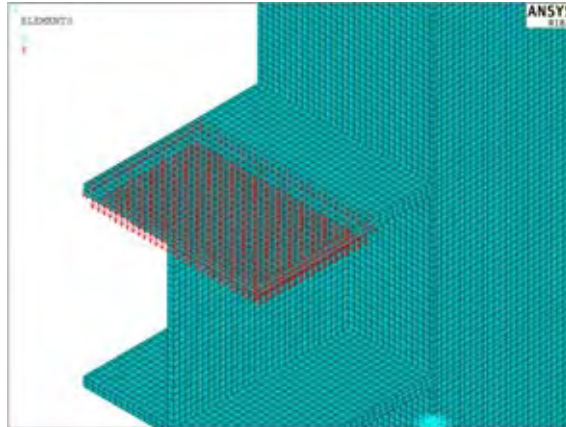


Figure 3.3 Loading condition of the model.

(2.) Boundary Conditions.

Since the column have 1 m length, the boundary conditions were restrained in all x-y-z directions at the bottom column end and only the x-y in-plane directions at the top column end. Figure 3.4 illustrated boundary condition of the column.

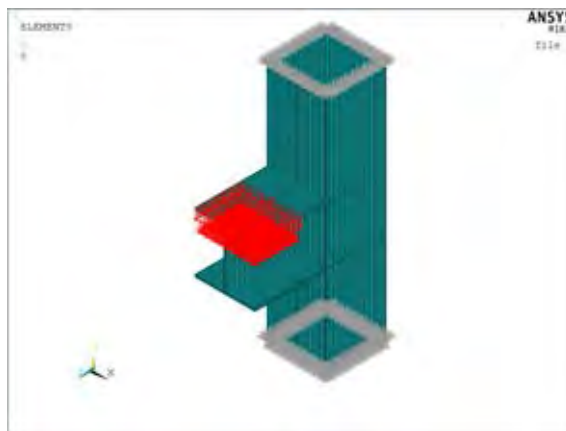


Figure 3.4 Boundary condition of the column.

2. Plastic Analysis Implementation.

2.1 Non-linear Finite Element Analysis.

The nonlinear push-over FE analyses adopted the Arc-Length Approach algorithm available directly in an ANSYS modeling system, where some specific parameters were set to 0.1% of equilibrium convergence criterion and more than 1000 load incremental substeps. Time at end of load step is equal to the crane load that applied to the model. The material properties assumed bilinear stress-strain,

namely elastic and perfectly plastic, constitutive laws. Large deformations were incorporated. The advantage of this method involves the tracing of a complex path in the load-displacement response into the post buckling regimes when the slope is become negative value.

The analysis procedures were performed in step-by-step fashions. Each step analysis assigned an updated positive-sign load factor (α) multiplied to the whole applied forces, varying from $\alpha = 0, 0.001$, and so on. The maximum load multiplier or safety factor α_{NL} in a more familiar engineering sense was determined from the maximum value of α that can be safely applied to structure.

The size of the incremental load factor $\Delta\alpha$ applied to the forces in the next step analysis is largely problem dependence. The smaller incremental load step yields the better equilibrium convergence and thus more accurate response solutions at the costs of more computing resources. Vice versa, the bigger step quickly performs the full structural responses, but is likely to experience the numerical instability or even divergence of equilibrium solutions. Some of HSS column can resist this crane capacity, crane loads that applied in the model from section 1.4 will be increased until the solution reached bifurcation point and continues to post buckling behavior.

3. Retrofit of Hollow-Section Columns.

3.1 Internal Plate Fabrication Strengthening

In this thesis, the internal plate fabrication will be analyzed with three-dimensional solid element (SOLID185). The material properties of stiffener plate employed were modulus of elasticity of 200,000 MPa, Poisson's ratio of 0.3 and yield stress of 250 MPa. The nonlinear FE analysis model for stiffener plate assumed bilinear elastic and perfectly plastic material properties. The stiffener plate is construct at the center of beam connection flange. The analyses considered the responses of stiffened HSS columns for various plate thicknesses, ranging from 3 mm

to the thickness of flange in connection beam for internal fabrications. The geometry of an internal plate fabrication displayed in Figure 3.5.

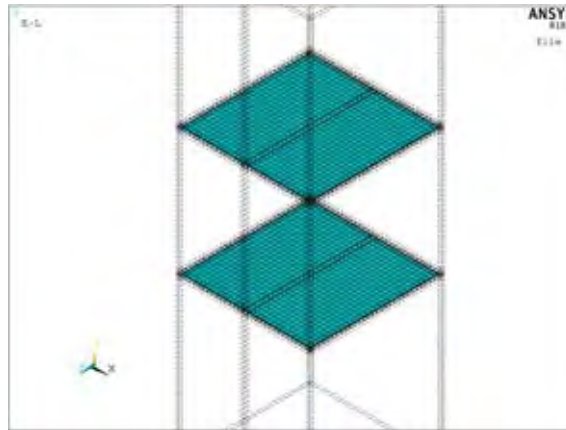


Figure 3.5 Geometry of internal plate fabrication.

3.2 External Ring Stiffener Strengthening

The external ring stiffener is modeled to improve the plastic capacity of the columns. Three-dimensional solid element (SOLID185), material properties of stiffener plate employed were modulus of elasticity of 200,000 MPa, Poisson's ratio of 0.3 and yield stress of 250 MPa also used to analyze the non-linear analysis. The thickness of external ring stiffener is same as the internal plate fabrication. External ring stiffeners having typical dimension of 100 mm width. Geometric of external ring stiffener displayed in Figure 3.6. The main idea of this strengthening technique is wanting to compare with the internal plate fabrication.



Figure 3.6 Geometry of external ring stiffener

CHAPTER 4 Results and Discussions

4.1 Comparison of Numerical Results with Experimental reference

Table 1 shows the numerically determined maximum load capacity for the uniplanar connection was compared with the experimental results from Fujiwara et al. (1981) by selecting cases where β is equal to 1. The results of the comparison are given in **Error! Not a valid bookmark self-reference..**

Table 3 Comparison of the numerical results with experimental reference.

Test specimens	Chord $b_0 \times h_0 \times t_0$ (mm)	I-beam $h_1 \times b_1 \times t_w \times t_1$ (mm)	2γ	f_{y0} (N/mm ²)	$M_{u,exp}$ (KNm)	$M_{u,FEM}$ (KNm)
H3	200x200x6	300x200x6x9	33.3	383	91.6	83.1
H4	200x200x6	400x200x8x13	33.3	383	106.7	111.3
H7	200x200x9	300x200x6x9	22.2	340	137.7	142
H10	200x200x12	300x200x6x9	16.7	378	187.0	197.55

4.2 Results before strengthening

The nonlinear FE analysis approaches were successfully performed to trace the complete load and displacement responses of all the column cases. The load–deflection curves for all columns are plotted in Figure 4.1. The deflection that was vertical in the Y-axis direction result was tracked at end of the corbels. Figure 4.2 illustrates the behavior of SHS 250x12 at different loadsteps. The equivalent stress (von-Mises stress) reached the yield stress, starting from the corner of the column that was attached to the flange of the beam connection, as depicted in Figure 4.2(a). The distribution of von-Mises stress moved to the center of the face of the columns along the flange in a horizontal line, as displayed in Figure 4.2(b) and Figure 4.2(c). The von-Mises stress continued to be distributed along the corner of the column in a vertical direction and was matched together, as shown in Figure 4.2(d) and Figure 4.2(e). Additionally, the von-Mises stress was distributed until the whole face of the

columns reached the yield stress, as displayed in Figure 4.2(f). Next, Figure 4.2(g) and Figure 4.2(h) illustrate that the column began to fail in the tension and compression zones at the top and bottom flanges, respectively. Finally, the von-Mises stress was further distributed to the end of both side walls and extended to yield stress which became the maximum load carrying capacity, as depicted in Figure 4.2(i).

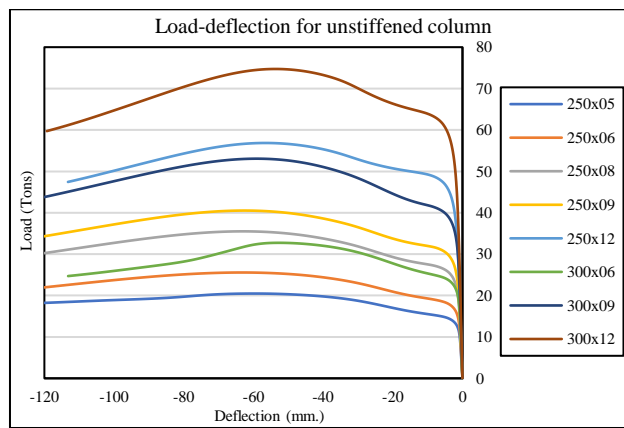


Figure 4.1 Load-deflection for the column without a stiffener.

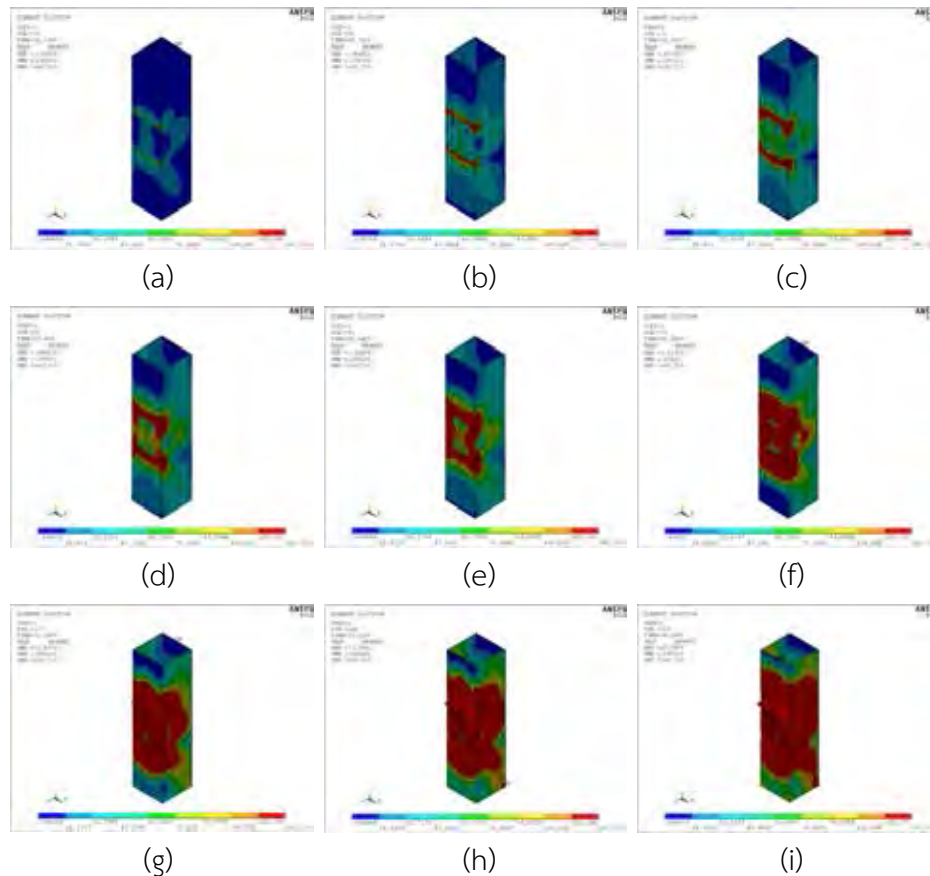


Figure 4.2 Equivalent stress along the column 250x12 at different loadsteps.

The maximum plastic capacity of the column is shown in **Error! Reference source not found.**. This result shows the load collapse for non-linear analysis (α_{NL}) by using the maximum nominal load step at the slope of the load-deflection curve equal to zero from the arc-length method, divided by the safety factor 1.67 to follow the specification code (ASD method). The result shows the maximum nominal capacity with the AISC design guide (ASD method) which provided the maximum axial compression and flexural strength for the box section. The load collapse from AISC (α_{AISC}) can be computed from Eq. (15).

Table 4 Comparison between α_{NL} and α_{AISC} without the strengthening technique.

Column	Non-linear FE (Factored)			AISC (ASD method)		
	Max. Load (KN)	Moment (KN-m)	α_{NL}	Compression (KN)	Moment (KN-m)	α_{AISC}
250x05	122.641	24.528	0.454	642.223	49.999	0.505
250x06	153.084	30.617	0.567	794.700	67.738	0.671
250x08	212.627	42.523	0.787	1044.467	95.093	0.927
250x09	242.671	48.534	0.899	1166.541	105.539	1.030
250x12	340.447	68.087	1.261	1520.960	132.777	1.334
300x06	196.024	39.205	0.726	928.577	86.386	0.779
300x09	317.725	63.545	1.177	1424.050	155.092	1.420
300x12	447.489	89.496	1.657	1864.721	197.218	1.813

From the results in **Error! Reference source not found.**, columns 250x05 and 300x06 after computing their width to thickness ratios (λ) were classified as slender-element sections to be subject to axial compression and its flanges member when considering flexure. Column 250x06 was classified as a compact section to be subject to axial compression but non-compact in flanges member when cogitate about members subject to flexure. Beyond these results, the columns were classified as compact sections to be subject to both axial compression and flexure.

These results clearly show that if the column width is equal, the thin columns will have α_{NL} less than the thick columns. For the columns with an equal thickness size, the large size of the column has the result of α_{NL} more than the small sized columns.

Error! Not a valid bookmark self-reference. shows α_{NL} by using the maximum nominal load step without dividing the safety factor at the deformation limit equal to $3\%b_0$, compared with the load collapse (α_{ref}) computed by Lu (1997) which was previous mentioned in Section 4.4 in Chapter 2. The load collapse α_{ref} was selected as the minimum moment capacity and was calculated from Eq. (16) and Eq. (17). Eq. (18) is not relevant for the connections considered in this work. The columns which were classified as non-compact and slender-element sections to be subject to axial compression and its flanges members are out of the validity range.

Table 5 Comparison between α_{NL} and α_{ref} without the strengthening technique

Column	Non-linear FE (Nominal)			Lu (1997)		
	Max. Load (KN)	Moment (KN-m)	α_{NL}	Eq. (16) (KN-m)	Eq. (17) (KN-m)	α_{ref}
250x05	15.195	30.39	0.563	20.219	21.313	0.242
250x06	18.923	37.846	0.701	27.633	30.691	0.331
250x08	27.077	54.154	1.003	45.830	54.562	0.539
250x09	31.509	63.018	1.167	56.615	69.055	0.660
250x12	48.501	97.002	1.796	95.704	122.763	1.030
300x06	25.137	50.274	0.931	36.167	36.598	0.401
300x09	41.576	83.152	1.540	72.333	82.346	0.733
300x12	63.545	127.09	2.354	120.556	146.392	1.209

4.3 Results for Internal Plate Fabrication

After performing the strengthening technique, it is clearly evidenced that the process enhanced the overall load carrying capacities of the stiffened columns compared to the unstiffened columns. As expected, thicker stiffening plates

increased the maximum retrofitted column strength. Figure 4.3 to Figure 4.10 plot the load-deflection curve for all the columns according to the varying stiffener thickness. The results show that thin columns with thin stiffener plates failed in the tension zone. In contrast, thin columns with thick stiffener plates failed in the compression zone. Thickening the stiffener plate thickener so that it was greater than a threshold did not further improve the column strength. The local failure occurred in the tension zone so long as the column was thick enough. For column section 250x05, the maximum load capacity compared with the unstiffened column with 11 mm stiffening was improved considerably by around 210 percent that closed to section 250x06. For column section 250x08, the maximum load capacity compared between the unstiffened and the 11 mm stiffening was improved by 180 percent. For column section 250x09, the maximum load capacity compared between the unstiffened and the 11 mm stiffened increase by 167 percent. For column section 250x12, the maximum load capacity compared between the unstiffened and the 11 mm stiffened was enhanced by around 116 percent.

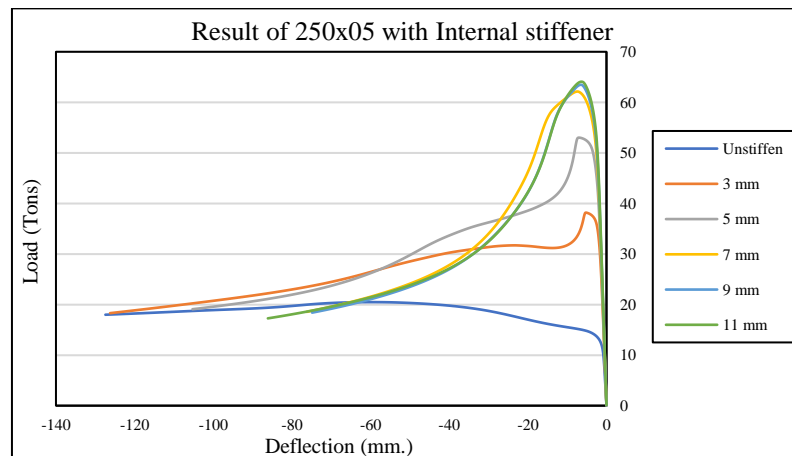


Figure 4.3 Result of 250x05 with internal stiffener

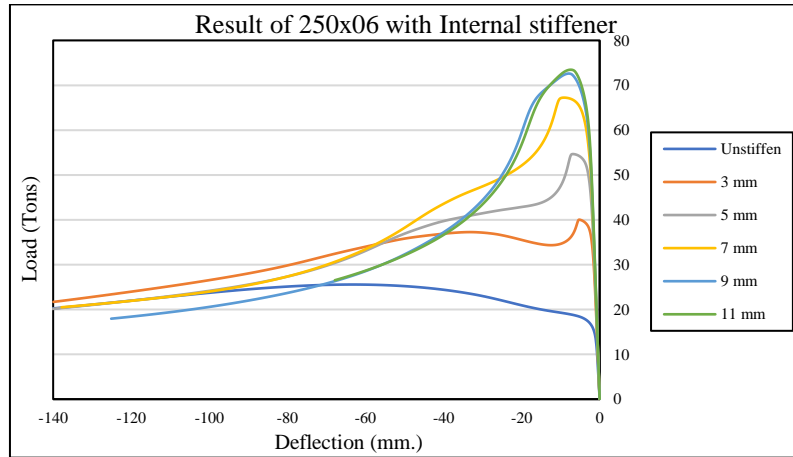


Figure 4.4 Result of 250x06 with internal stiffener.

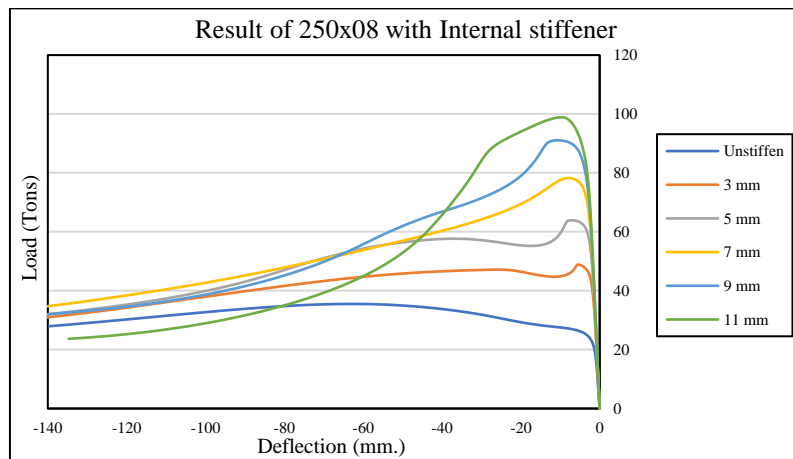


Figure 4.5 Result of 250x08 with internal stiffener

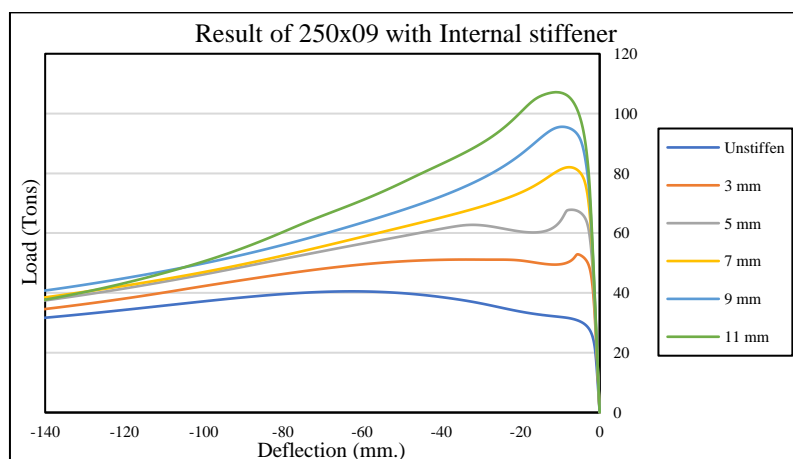


Figure 4.6 Result of 250x09 with internal stiffener



1413517646

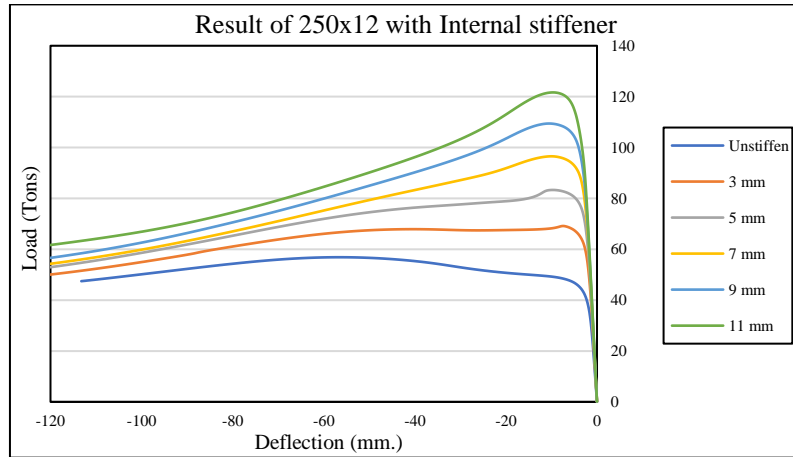


Figure 4.7 Result of 250x12 with internal stiffener

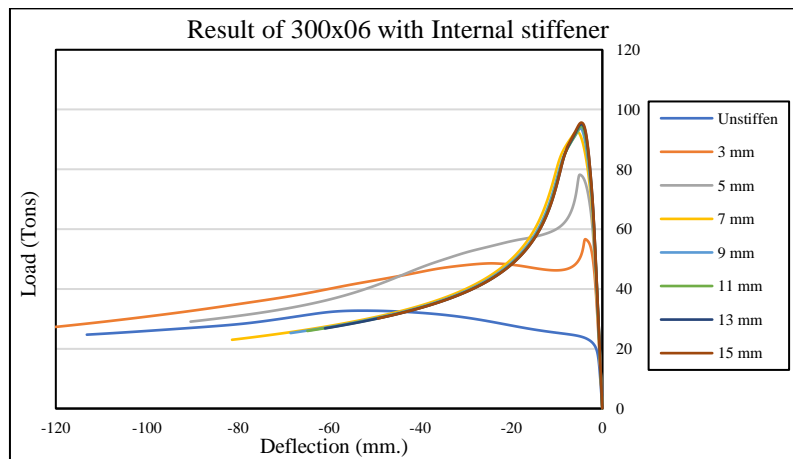


Figure 4.8 Result of 300x06 with internal stiffener

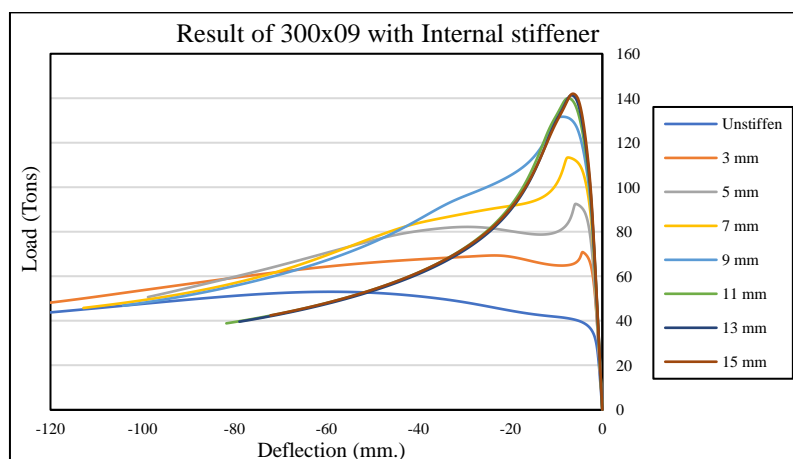


Figure 4.9 Result of 300x09 with internal stiffener



1413517646

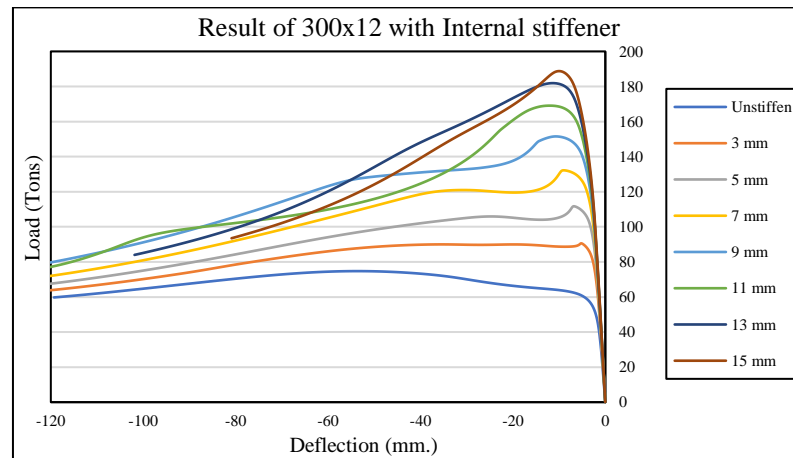


Figure 4.10 Result of 300x12 with internal stiffener

Figure 4.11 to Figure 4.13 depict the distribution of von Mises stresses for an internal plate stiffened in column section 300x06 under applied crane forces. These describe the local buckling failures of columns and the stress distribution underpinning the stiffener plates. The results show that different stiffener plate thicknesses will cause different column failure behaviors.

Figure 4.11(a) shows that the von-Mises stress became a yield stress starting at the corner of the column. The distribution of von-Mises stress continued to develop along the flange of corbel in a horizontal line, as displayed in Figure 4.11(b). Figure 4.11(c) illustrates that the von-Mises stress reached yield stress and then move forward into a vertical direction along the web until it matched together and reached its maximum capacity. Next, the stress spread up to the whole face of the columns, as shown in Figure 4.11(d) and Figure 4.11(e). Finally, Figure 4.11(f) shows that the column had a local failure at the tension zone when a 3 mm thick internal stiffener was used. One observation of this result is that the whole column does not need to reach yield stress to get the maximum load capacity. This is because the von-Mises stress was distributed to the stiffener plate inside the column.

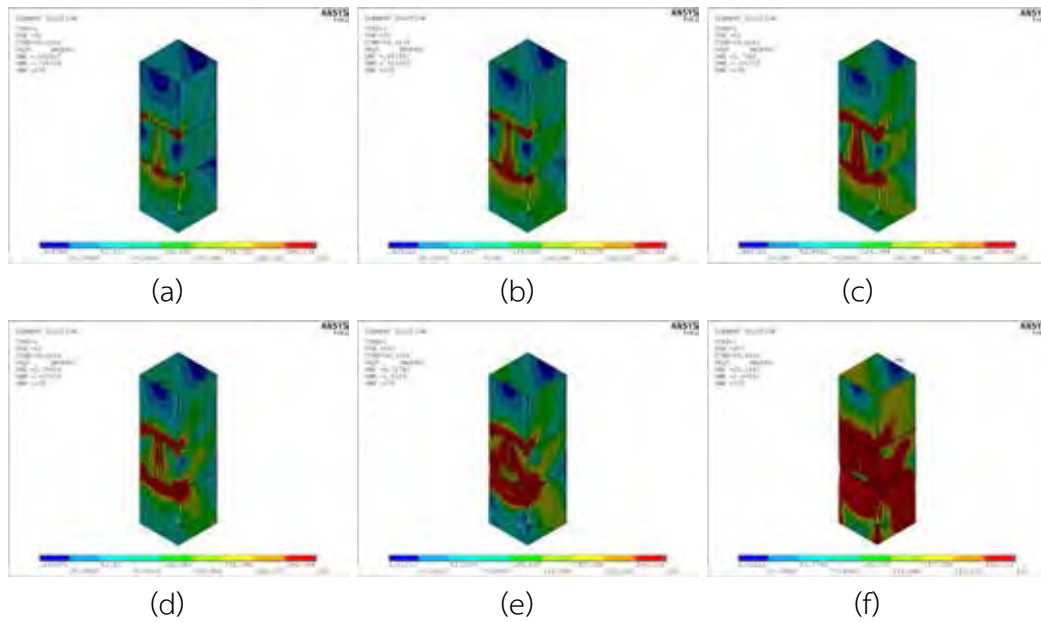


Figure 4.11 Result of 300x06 with a 3 mm thick internal stiffener plate.

The behavior of column 300x06 with a 5 mm internally stiffener was similar to the 3 mm thickness. It is observed that when the column had a width to thickness ratio (λ) classified as a slender element for both axial compression and flexure, the failure occurred in the tension zone if the stiffener plate was not thick enough.

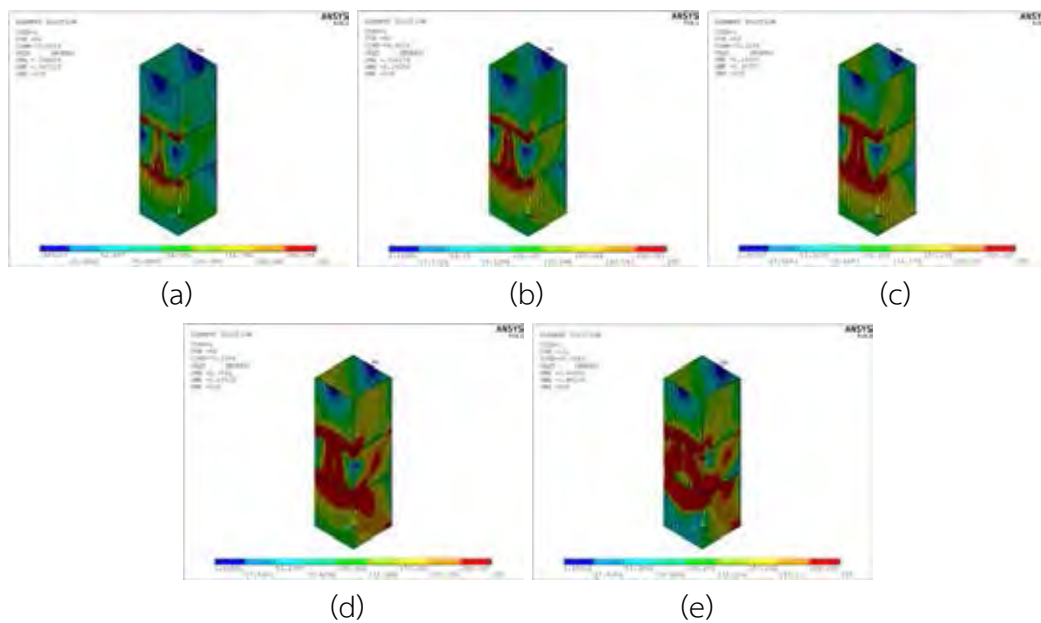


Figure 4.12 Result of 300x06 with a 5 mm thick internal stiffener plate.

For column 300x06 with a 9 mm thick internal stiffener plate, the von-Mises stress distributed along the horizontal direction along the flange of corbel then continued into a vertical direction along the web, as shown in Figure 4.13(a) and Figure 4.13(b). Figure 4.13(c) shows that the von-mises stress continued to spread widely around the column until reaching the maximum load carrying capacity. After that, the stress began moving underneath the stiffener plate in the compression zone and continued to develop until the whole of the column reached its yield stress, as displayed in Figure 4.13(d). Finally, Figure 4.13(e) clearly shows that the column failed in the compression zone. One further observation is that the column which had a slender element for both axial compression and flexure had a failure occurring in the compression zone if the stiffener plate was thick enough.

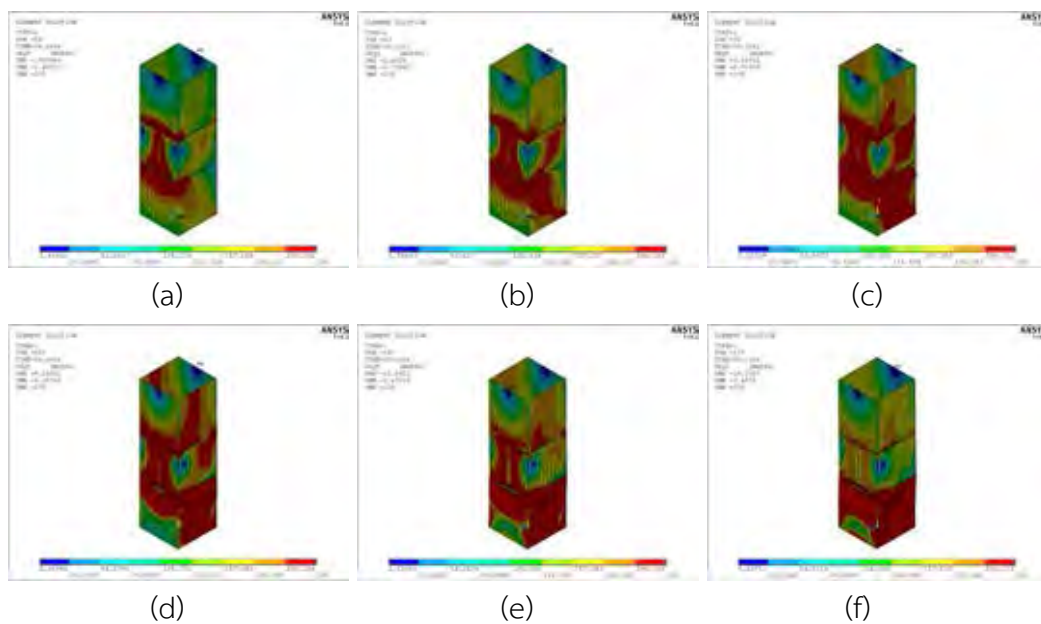


Figure 4.13 Result of 300x06 with a 9 mm thick internal stiffener.

4.4 Results for External Ring Stiffener

The external ring stiffener technique can slightly improve the maximum load capacity of the columns. The result of load-displacement in a vertical direction at the end of the corbels were plotted graphically in Figures Figure 4.14 to Figure 4.21. The results clearly show that most of the external ring stiffener techniques give the

behavior result to fail at the tension zone. For example, the column width 250 with a thickness from 6 to 12 mm failed in the tension zone, except for where the thickness was equal to 5 mm with a 11 mm stiffener plate, where the local failure occurred in the compression zone and had low ductility. For column section 250x05, the maximum load capacity compared between the unstiffened column and the column with 11 mm external stiffening increased significantly by around 164 percent. For column section 250x06, the maximum load capacity compared between the unstiffened and the 11 mm external stiffened columns improved by around 132 percent. For column section 250x08, the maximum load capacity compared between the unstiffened and the 11 mm external stiffened columns enhance by around 94 percent. For column section 250x09, the maximum load capacity compared between the unstiffened and the 11 mm external stiffened columns rose by 82 percent. For column section 250x12, the maximum load capacity compared between the unstiffened and the 11 mm external stiffened columns was boosted by 59 percent.

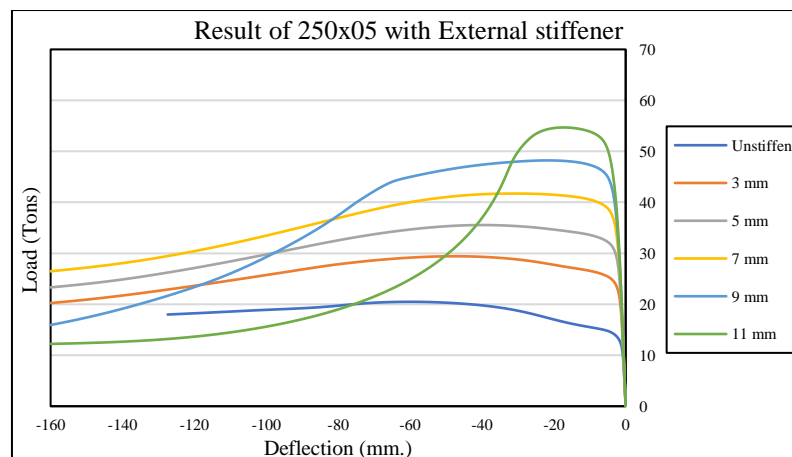


Figure 4.14 Result of 250x05 with external stiffener

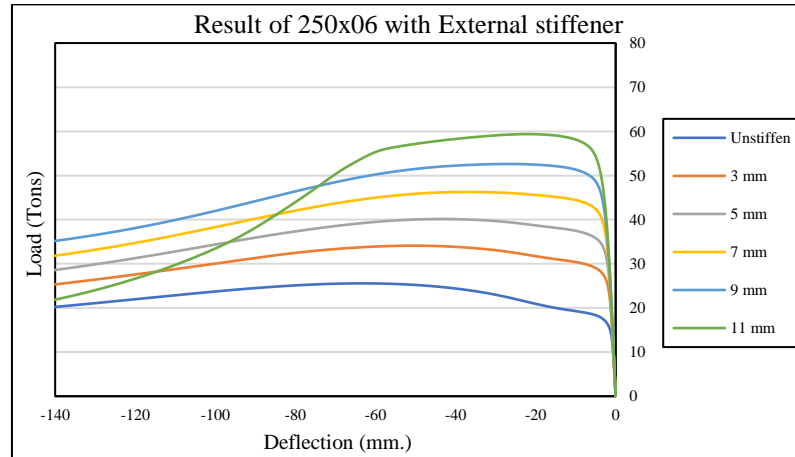


Figure 4.15 Result of 250x06 with external stiffener

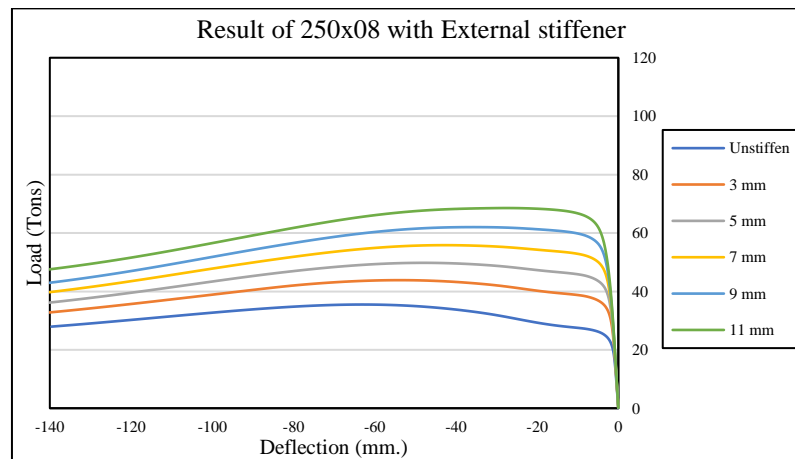


Figure 4.16 Result of 250x08 with external stiffener

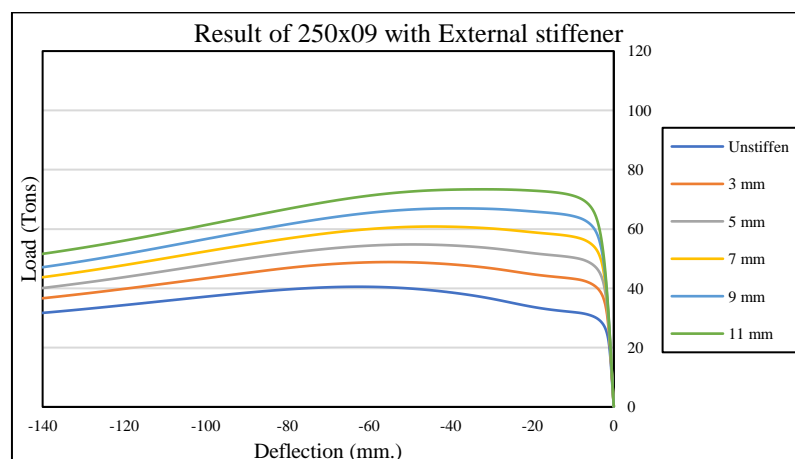


Figure 4.17 Result of 250x09 with external stiffener



1413517646

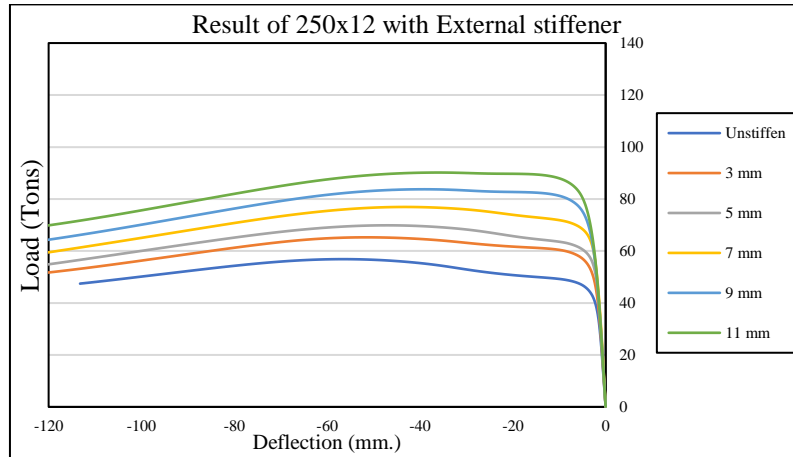


Figure 4.18 Result of 250x12 with external stiffener

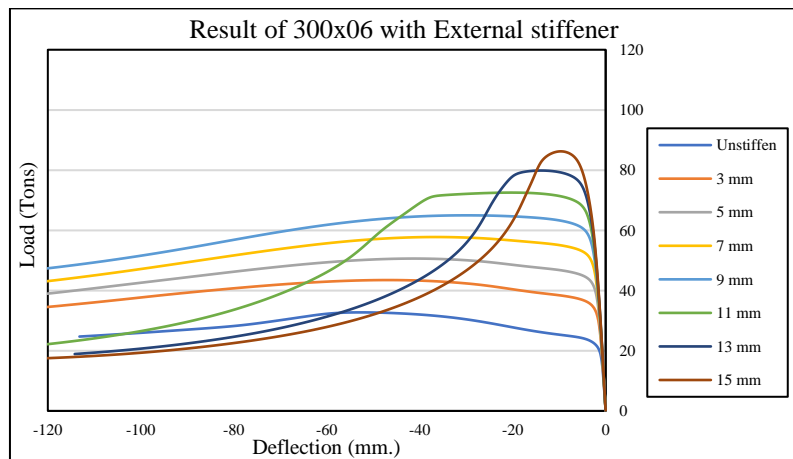


Figure 4.19 Result of 300x06 with external stiffener

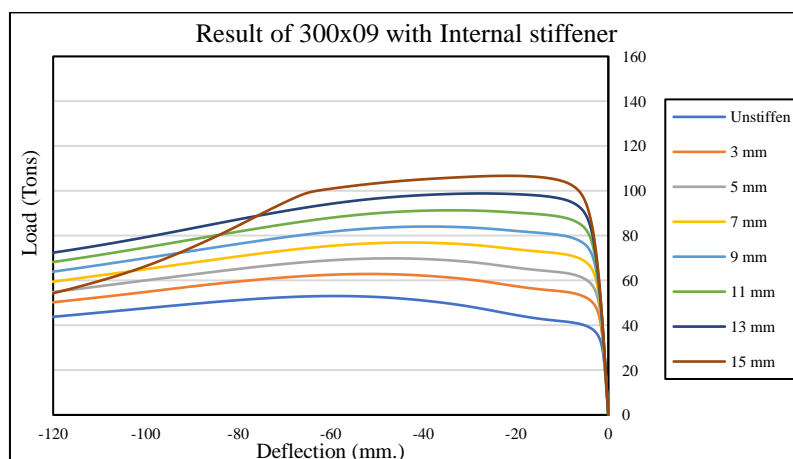


Figure 4.20 Result of 300x09 with external stiffener

1413517646

CD :thesis 6070287021 thesis / rev: 01082562 19:12:57 / seq: 13

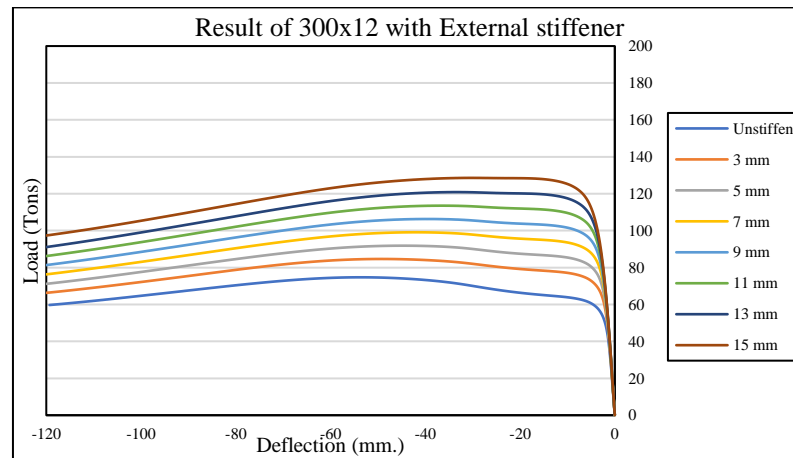


Figure 4.21 Result of 300x12 with external stiffener

A series of Figure 4.22 to Figure 4.23 depict the distribution of von Mises stresses for an external ring stiffening for column section 300x06 under applied crane forces. These describe the local buckling and post buckling failure behaviors of the columns and the stress distribution underpinning the stiffener ring. The results show that the different stiffener ring thicknesses cause different column failure behaviors.

According to Figure 4.22(a) and Figure 4.22(b), the result of column 300x06 with an external stiffener with a 9 mm thick plate showed that the von-Mises stress was distributed from the corner of the column to center of the face in a horizontal line along the flange, and along a vertical line along a web of corbel, similar to the internal plate stiffener. The von-Mises stress continued to spread widely from the web until whole face of the column reached the yield stress, as depicted in Figure 4.22(c) and Figure 4.22(d). The difference between the two strengthening techniques is that the external ring stiffener must have the yield stress distributed fully face of the column to reach the maximum load carrying capacity, as displayed in Figure 4.22(e). Finally, for the post buckling behavior, Figure 4.22(f) clearly shows that the column failed in the tension zone.

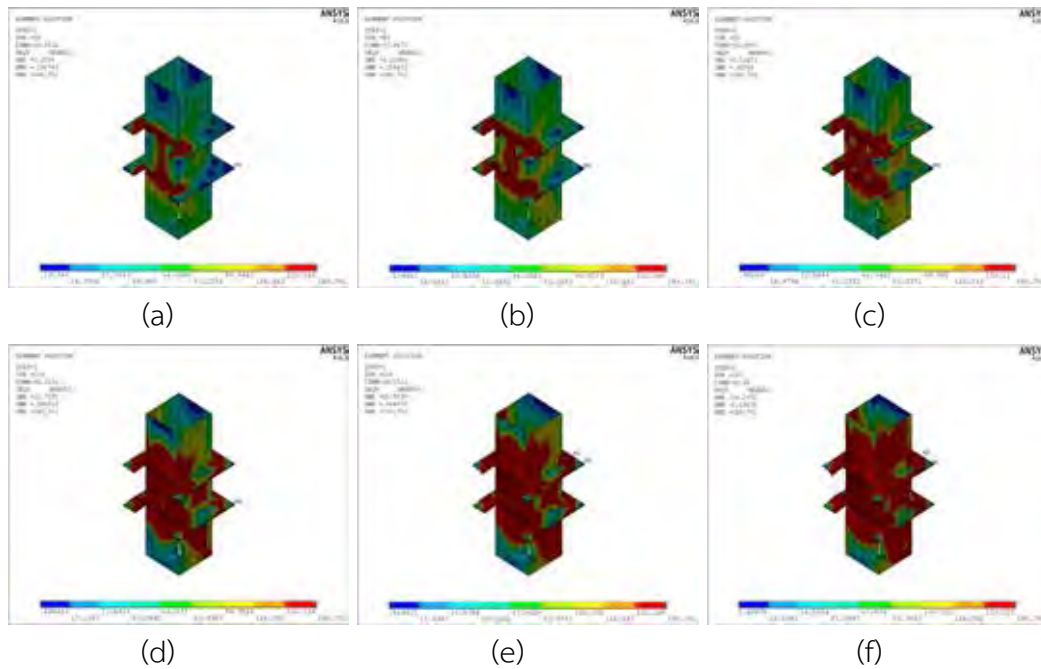
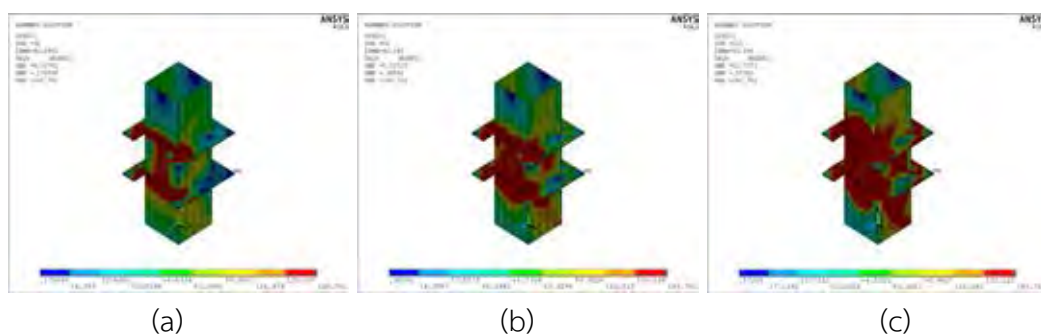


Figure 4.22 Result of 300x6 with a 9 mm thick external stiffener plate.

From Figure 4.23(a) to Figure 4.23(d), the von-Mises stress distribution are the same as Figure 4.22(a) to Figure 4.22(e) until reaching the maximum load capacity. After that, the von-Mises stress slightly moves to underneath the stiffener ring at the compression zone. Finally, Figure 4.23(f) illustrates that the column failed in the compression zone when the stiffener plate was thick enough. One observation from this result is that the column with a slender element for both axial compression and flexure had the failure occurring in the compression zone if the stiffener plate was thick enough, the same as the internal plate stiffener. The ductility of the post-buckling behavior would decrease if the stiffener plate thickness is increased.



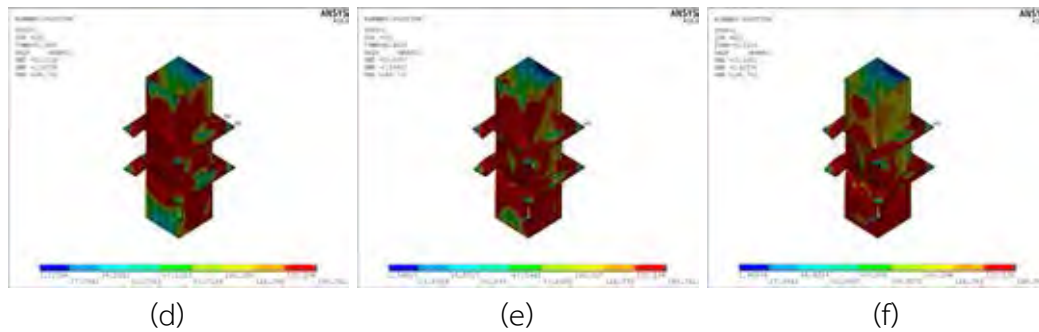


Figure 4.23 Result of 300x06 with an 11 mm thick external stiffener plate.

4.5 Summary of Results

The nonlinear push over FE analysis adopted the arc-length method were successfully performed to discover the complete load and displacement responses of all the column cases. The results illustrate that the more effective retrofitting method uses internally connected steel plates of the HSS columns, compared with the external ring fabrications. As expected, thicker stiffening plates resulted in a higher maximum retrofitted column strength, as described in **Error! Not a valid bookmark self-reference.** and Table 7. The increases plate thickness—described in Figure 4.24 and Figure 4.25 for the internal plate stiffening—converged to some certain maximum values of the column load capacity. For the external plate stiffening, increased plate thickness was found to slightly increase the maximum load capacity. When comparing the two strengthening techniques, internal plate stiffening fabrication was found to be more effective than the external ring type.

Table 6 Load collapse at the maximum capacity of the internal stiffener.

Stiffener Thickness (mm)	α_{NL} (SHS 250x05)		α_{NL} (SHS 250x06)		α_{NL} (SHS 250x08)		α_{NL} (SHS 250x09)	
	Unstiffened	Stiffened	Unstiffened	Stiffened	Unstiffened	Stiffened	Unstiffened	Stiffened
3	0.759	1.414	0.947	1.482	1.315	1.811	1.501	1.960
4		1.697		1.757		2.093		2.240
5		1.964		2.024		2.367		2.512
6		2.186		2.275		2.635		2.777
7		2.301		2.490		2.898		3.039
8		2.335		2.632		3.149		3.295
9		2.351		2.689		3.372		3.540

10		2.363		2.710		3.543		3.763
11		2.373		2.721		3.662		3.968
Stiffener Thickness (mm)	α_{NL} (SHS 250x12)		α_{NL} (SHS 300x06)		α_{NL} (SHS 300x09)		α_{NL} (SHS 300x12)	
	Unstiffened	Stiffened	Unstiffened	Stiffened	Unstiffened	Stiffened	Unstiffened	Stiffened
3	2.106	2.561	1.212	2.098	1.965	2.625	2.768	3.353
4		2.827		2.502		3.031		3.748
5		3.085		2.896		3.427		4.137
6		3.332		3.265		3.817		4.520
7		3.575		3.431		4.199		4.896
8		3.816		3.455		4.565		5.259
9		4.053		3.471		4.846		5.612
10		4.284		3.486		5.093		5.949
11		4.505		3.500		5.186		6.262
12		-		3.512		5.217		6.529
13		-		3.522		5.235		6.737
14		-		3.531		5.247		6.878
15		-		3.542		5.260		6.991

Table 7 Load collapse at the maximum capacity of the external stiffener.

Stiffener Thickness (mm)	α_{NL} (SHS 250x05)		α_{NL} (SHS 250x06)		α_{NL} (SHS 250x08)		α_{NL} (SHS 250x09)					
	Unstiffened	Stiffened	Unstiffened	Stiffened	Unstiffened	Stiffened	Unstiffened	Stiffened				
3	0.759	1.090	0.947	1.263	1.315	1.624	1.501	1.809				
4		1.203		1.375		1.734		1.919				
5		1.316		1.487		1.844		2.029				
6		1.431		1.601		1.956		2.141				
7		1.545		1.714		2.068		2.253				
8		1.666		1.831		2.182		2.367				
9		1.786		1.949		2.297		2.480				
10		1.906		2.074		2.418		2.599				
11		2.025		2.199		2.539		2.718				
Stiffener Thickness (mm)		α_{NL} (SHS 250x12)		α_{NL} (SHS 300x06)		α_{NL} (SHS 300x09)		α_{NL} (SHS 300x12)				
		Unstiffened		Stiffened		Unstiffened		Stiffened	Unstiffened	Stiffened	Unstiffened	Stiffened
3	2.106	2.417	1.212	1.610	1.965	2.329	2.768	3.136				
4		2.502		1.743		2.458		3.266				
5		2.588		1.875		2.588		3.402				

6		2.719		2.007		2.718		3.536
7		2.849		2.140		2.849		3.671
8		2.976		2.273		2.981		3.804
9		3.102		2.407		3.113		3.937
10		3.221		2.547		3.247		4.072
11		3.340		2.687		3.382		4.205
12		-		2.822		3.521		4.341
13		-		2.958		3.661		4.477
14		-		3.076		3.806		4.619
15		-		3.194		3.952		4.763

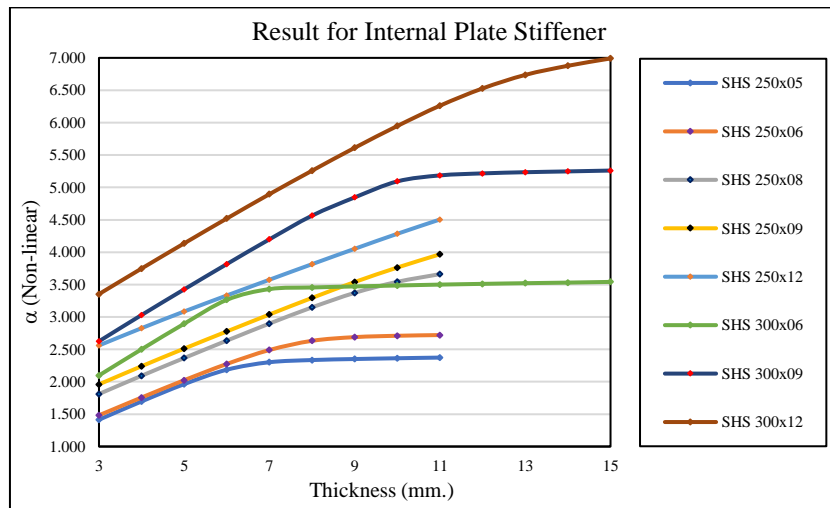


Figure 4.24 Graph of internal stiffener between α_{NL} and plate thickness.

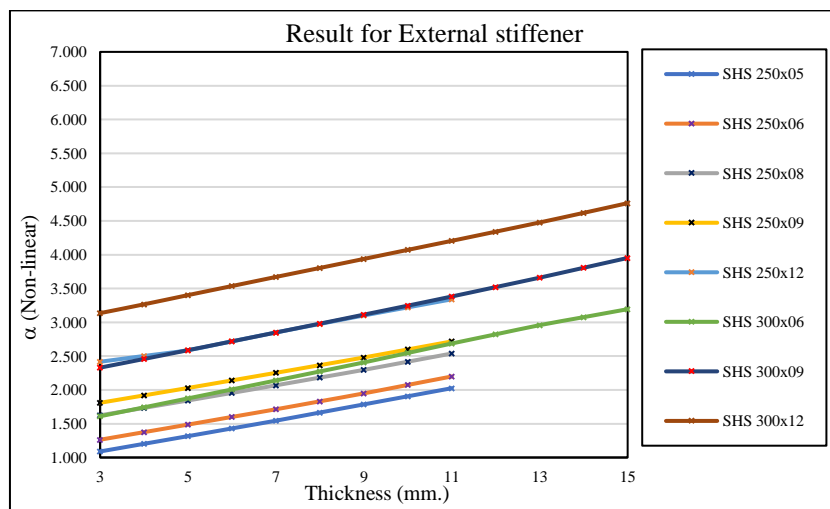


Figure 4.25 Graph of external stiffener between α_{NL} and plate thickness.



CHAPTER 5 Conclusion

This thesis presents the analysis and design of steel SHS column stiffening methods using steel plates. Two stiffening procedures—the internal and external-ring plate fabrications—were studied. The nonlinear FE analyses, considering the influence of inelastic materials and large deformations simultaneously, were successfully completed, and the results for the complete column responses under industry crane loads were computed. The present study is underlined by the application of an efficient column design for general warehouses.

The response solutions fruitfully provide the maximum load carrying capacity or safety factor for both the unstiffened and stiffened columns under applied forces. These also show the column capacity enhancement with the use of steel stiffening plates. Thicker stiffening plates resulted in greater column strength. Internal plate stiffening fabrication is more effective than the external ring type. Moreover, increasing the plate thickness was found to improve the overall column loading capacity, and converges to some certain threshold, after which increasing the plate thickness does not result in further column strength improvements.

REFERENCES

Ahmadi, H., et al. (2012). "Parametric study and formulation of outer-brace geometric stress concentration factors in internally ring-stiffened tubular KT-joints of offshore structures." Applied Ocean Research **38**: 74-91.

AISC (2016). Specification for Structural Steel Buildings, American National Standard ANSI/AISC 360-16.

AISI (2012). North American specification for the design of cold-formed steel structural members.

ANSYS, I. (2017). ANSYS Mechanical APDL Element Reference, Southpointe 2600 ANSYS Drive Canonsburg, PA 15317

Bauccio, M. (1993). ASM metals reference book. United States of America, ASM international.

BOEL, H. (2010). Buckling length factors of hollow section members in lattice girders. Eindhoven University of Technology.

Cao, S., et al. (2018). "Experimental seismic behaviour of bottom-through-diaphragm and top-ring connection to SST columns." Journal of Constructional Steel Research **150**: 249-260.

Chang, H., et al. (2014). "Compression behavior of doubler-plate reinforced square hollow section T-joints." Adv. Steel Constr. Inter. J **10**(3): 289-309.

Chen, L., et al. (2008). "Limit analysis of structures containing flaws based on a modified elastic compensation method." European Journal of Mechanics-A/Solids **27**(2): 195-209.

Crisfield, M. A. (1981). A fast incremental/iterative solution procedure that handles "snap-through". Computational Methods in Nonlinear Structural and Solid Mechanics, Elsevier: 55-62.

De Winkel, G. D. (1998). The static strength of i-beam to circular hollow section column connections. Ph.D. Dissertation, Delft University of Technology, Delft, The Netherlands.

Garifullin, M., et al. (2017). "Initial in-plane rotational stiffness of welded RHS T joints with axial force in main member." Journal of Constructional Steel Research **139**: 353-362.

Henriques De Sena Cardoso, F. M. (2015). "System reliability-based criteria for designing cold-formed steel structures by advanced analysis."

Jones, R. M. (2009). Deformation theory of plasticity. Virginia, United State, Bull Ridge Corporation.

Kanatani, H., et al. (1981). "Bending tests on T-joints of RHS chord and RHS or H-shape branch." CIDECT Program 5AF.

Kurobane, Y. (2004). Design guide for structural hollow section column connections, Verlag TUV Rheinland.

Lee, M. and A. Llewelyn-Parry (2004). "Offshore tubular T-joints reinforced with internal

plain annular ring stiffeners." Journal of Structural Engineering **130**(6): 942-951.

Lee, M. M. and A. Llewelyn-Parry (1999). "Strength of ring-stiffened tubular T-joints in offshore structures—: a numerical parametric study." Journal of Constructional Steel Research **51**(3): 239-264.

Lu, L. H. (1997). The static strength of I-beam to rectangular hollow section column connections, Delf University, Netherland.

MACCRIMMON, R. (2009). "CRANE-SUPPORTING STEEL STRUCTURES." Canadian Institute of Steel Construction.

Mackenzie, D. and J. Boyle (1992). "A method of estimating limit loads by iterative elastic analysis. I—Simple examples." International Journal of Pressure Vessels and Piping **53**(1): 77-95.

Mackenzie, D., et al. (1994). "Finite element modelling for limit analysis by the elastic compensation method." Computers & structures **51**(4): 403-410.

Madenci, E. and I. Guven (2015). The finite element method and applications in engineering using ANSYS®, Springer.

Mangat, P. (1969). Influence of the slenderness and b/t ratios on the inelastic local buckling of angles, University of Windsor (Canada). **Master of Applied Science in Civil Engineering**.

MBMA (2012). Metal Building Systems Manual, Base on the 2012 IBC and ASCE 7-10.

Nadarajah, C., et al. (1992). "A method of estimating limit loads by iterative elastic analysis. II—Nozzle sphere intersections with internal pressure and radial load." International Journal of Pressure Vessels and Piping **53**(1): 97-119.

Nadarajah, C., et al. (1996). "Limit and shakedown analysis of nozzle/cylinder intersections under internal pressure and in-plane moment loading." International Journal of Pressure Vessels and Piping **68**(3): 261-272.

Packer, J. A. (1993). "Moment connections between rectangular hollow sections." Journal of Constructional Steel Research **25**(1-2): 63-81.

Riks, E. (1979). "An incremental approach to the solution of snapping and buckling problems." International journal of solids and structures **15**(7): 529-551.

Szlendak, J. (1991). "Beam-column welded RHS connections." Thin-Walled Structures **12**(1): 63-80.

T. Uraipong, K. P. (2016). Strength Enhancement of Connections between Steel I-Beam and Circular Hollow Steel Column by Nonlinear Finite Element Analysis. The 21st National Convention on Civil Engineering. Songkhla, THAILAND: 35-43.

Thepchatri, T. (2017). Behavior of Steel Structure, Civil Engineering Department, College of Engineering Chulalongkorn University.

Thompson, G. (2007). Best practice of crane support structures design: an expert survey, Stellenbosch: University of Stellenbosch.

Ting, L., et al. (1991). "Box-column to I-beam connections with external stiffeners." Journal of Constructional Steel Research **18**(3): 209-226.

Vigil, J. (2014). Structural steel design: a practice-oriented approach, Pearson.

Von Mises, R. (1913). "Mechanics of solid bodies in the plastically-deformable state." German.) Nachr. Ges. Wiss. Goettingen, Math.-Phys. Kl **1**: 582-592.

Voth, A. P. and J. A. Packer (2012). "Branch plate-to-circular hollow structural section connections. I: Experimental investigation and finite-element modeling." Journal of Structural Engineering **138**(8): 995-1006.

Wardenier, J. (1982). Hollow section joints. Civil Engineering and Geosciences, Delft University Press, Netherland. **Docoral thesis**.

Wardenier, J., et al. (2002). Hollow sections in structural applications, Bouwen met Staal Rotterdam,, The Netherlands.

Wu, J. (2013). Numerical modelling and optimization of new RHS column-to-I beam connections, Swansea University (United Kingdom).

Yang, P., et al. (2005). "Limit analysis based on a modified elastic compensation method for nozzle-to-cylinder junctions." International Journal of Pressure Vessels and Piping **82**(10): 770-776.

Yu, W.-W. (2000). Cold-formed steel design, John Wiley & Sons.

Yu, W.-W. and R. A. LaBoube (2010). Cold-Formed Steel Design, John Wiley & Sons.

Zhao, X.-L. (2000). "Deformation limit and ultimate strength of welded T-joints in cold-formed RHS sections." Journal of Constructional Steel Research **53**(2): 149-165.



1413517646

CU IThesis 6070287021 thesis / recv: 01082562 19:12:57 / seq: 13

VITA

NAME	Rut Su
DATE OF BIRTH	16 October 1994
PLACE OF BIRTH	Taipei Taiwan
INSTITUTIONS ATTENDED	B.Eng (Survey Engineering) Kasetsart University
HOME ADDRESS	72/72 Sathorn premier place condominium Prachao Thaksin road Bukkalo Thonburi Bangkok 10600
PUBLICATION	The 24th National Convention on Civil Engineering